

Geochronology, elemental and Nd–Hf isotopic geochemistry of Devonian A-type granites in central Jiangxi, South China: Constraints on petrogenesis and post-collisional extension of the Wuyi–Yunkai orogeny



Shang-Jie Feng ^a, Kui-Dong Zhao ^{a,b,c,*}, Hong-Fei Ling ^a, Pei-Rong Chen ^a, Wei-Feng Chen ^a, Tao Sun ^a, Shao-Yong Jiang ^{a,b,c}, Wei Pu ^a

^a State Key Laboratory for Mineral Deposits Research, School of Earth Sciences and Engineering, Nanjing University, Nanjing 210093, PR China

^b State Key Laboratory for Geological Processes and Mineral Resources, China University of Geosciences, Wuhan 430074, PR China

^c Faculty of Earth Resources and Collaborative Innovation Center for Exploration of Strategic Mineral Resources, China University of Geosciences, Wuhan 430074, PR China

ARTICLE INFO

Article history:

Received 10 February 2014

Accepted 11 July 2014

Available online 23 July 2014

Keywords:

A-type granite

Early-middle Paleozoic

Wuyi–Yunkai orogeny

South China

ABSTRACT

Details on processes of the early-middle Paleozoic Wuyi–Yunkai orogeny in South China remain poorly defined. Most Silurian–Devonian granites in South China are S-type or I-type granites, which are suggested to be petrogenetically related to the Wuyi–Yunkai orogeny. This paper firstly reported a systematic study on two Devonian A-type granites in the central Jiangxi Province. LA-ICP-MS zircon U-Pb dating results imply that the Huitong and Epo granites were emplaced at about 415 Ma. Both of the two granites have the petrographic and geochemical characteristics of A-type granites. Interstitial biotites occur along the boundary of euhedral plagioclase and quartz and they formed later than plagioclase and quartz. It implies that the primary magma could have been anhydrous. Biotites from the two granites are Fe-rich and have high $\text{Fe}^{2+}/(\text{Fe}^{2+} + \text{Mg}^{2+})$ ratios (0.60–0.74). The magmatic temperatures estimated from zircon saturation thermometer are 802–920 °C for the two granites, higher than common I-type and S-type granites. The two granites show high contents of total alkalis ($\text{Na}_2\text{O} + \text{K}_2\text{O} = 6.96\text{--}9.39$ wt.%), high field strength elements (e.g. $\text{Zr} = 181\text{--}437$ ppm, $\text{Y} = 22.1\text{--}39.7$ ppm, $\text{Nb} = 18.6\text{--}30.3$ ppm and $\text{Zr} + \text{Nb} + \text{Ce} + \text{Y} = 324\text{--}555$ ppm), rare earth elements (total REE = 155–312 ppm) as well as high Ga/Al ratios ($10,000 \times \text{Ga}/\text{Al} = 2.50\text{--}3.44$). These geochemical characteristics are similar to those of A-type granites. The Huitong and Epo granites have relatively low $\varepsilon_{\text{Nd}}(t)$ values of -10.4 to -7.7 , and low zircon $\varepsilon_{\text{HF}}(t)$ values (peak value of -8.0). Whole-rock two stage Nd isotopic model ages and zircon Hf isotopic model ages mostly vary from 1.78 Ga to 2.00 Ga. According to these data, we suggest that the two granites might have derived from partial melting of pre-Cambrian sedimentary rocks which had been granitized during an earlier thermal event. The two granites contain abundant contemporaneous mafic microgranular enclaves (MMEs). The MMEs display igneous textures and contain acicular apatites, suggesting quenching of mafic magmas that have co-mingled with the host granites. The MMEs might have derived from the enriched lithospheric mantle source. This study on the Devonian Huitong and Epo A-type granites, together with previous studies on Paleozoic granites in South China, indicated that the Wuyi–Yunkai orogeny in South China had changed from syn-collisional crustal thickening to post-collisional extension at least from 415 Ma.

© 2014 Elsevier B.V. All rights reserved.

1. Introduction

The South China Block (SCB), East Asia (Fig. 1), is a major continental block with a complex tectonic history. It is generally accepted that the SCB was formed by amalgamation of the Yangtze Block in the northwest and the Cathaysia Block in the southeast during Neoproterozoic time

(e.g. Charvet, 2013; Li et al., 2009). The unified SCB subsequently underwent at least three major tectono-thermal events, during the early-middle Paleozoic (traditionally named as “Caledonian”), the Triassic (Indosinian) and the Jurassic–Cretaceous (Yanshanian), respectively. An abundance of igneous rocks, especially granites, formed in response to these events, with the granites in the eastern SCB commonly regarded as one large granite province (Wang and Zhou, 2005). Despite intensive scientific research during the past half century, the geodynamic mechanism of these tectonic–magmatic events remains controversial, and a series of contrasting models, especially intra-plate orogeny and subduction of oceanic plate, have been suggested

* Corresponding author at: Room 186/20, School of Ocean and Earth Sciences, University of Southampton, European Way, SO14 3ZH Southampton, UK.

E-mail address: zhaokd@cug.edu.cn (K.-D. Zhao).

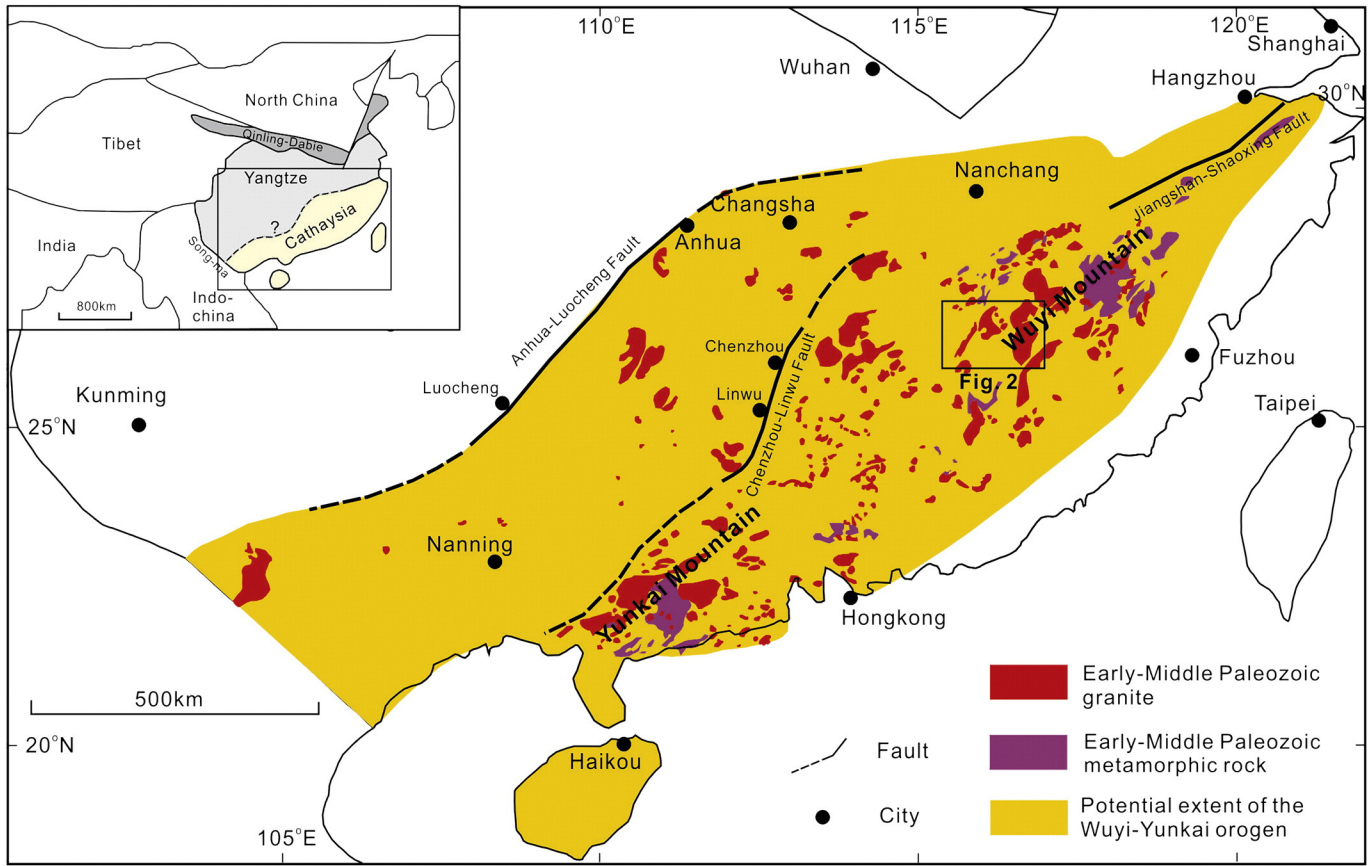


Fig. 1. Simplified geological map showing the distribution of the Paleozoic granites and high-grade metamorphic rocks in the eastern South China Block (modified from Li et al. (2010) and Zhao et al. (2013a)). The location of the Huitong and Epo plutons is shown in the map.

(e.g. Gilder et al., 1991; Hsü et al., 1988; Li and Li, 2007; Li et al., 2010; Wang et al., 2013a; Zhou and Li, 2000; Zhou et al., 2006).

The early-middle Paleozoic tectono-thermal event in South China is characterized by an angular unconformity between pre-Devonian deformed rocks and Devonian strata, and widespread high-grade metamorphic rocks, migmatites and granitoids (Charvet et al., 2010; Li et al., 2010; Wang et al., 2011, 2012; Xu et al., 2011; Yu et al., 2003, 2007; Zhao and Cawood, 1999). This unconformity has been suggested to result from a major intra-plate orogenic event due to the lack of an oceanic suture record (e.g. Charvet, 2013; Charvet et al., 2010; Faure et al., 2009; Li et al., 2010; Shu et al., 2008). This orogenic belt spans the southeastern half of the South China Block, stretching for ~2000 km length in a northeasterly direction (Fig. 1). The orogenic event was originally assigned to the Kwangssian movement (Ting, 1929), and has variously been named as the South China Caledonian Fold Belt (Huang, 1978), the Wuyishan–Yunkaidashan Belt (Zhang et al., 1984), and the early Paleozoic Orogen of the South China Block (Faure et al., 2009) by different investigators. Recently, Li et al. (2010) renamed it the Wuyi–Yunkai orogeny, but Wang et al. (2011, 2012, 2013a) still used the previous Kwangssian orogeny to define the event. The early Paleozoic high-grade metamorphic rocks which reach amphibolite to granulite facies occur mainly in the Wuyi Mountain and the Yunkai Mountain (Fig. 1). Hence, in order to show the lateral extent of this large orogeny, we recommend using the Wuyi–Yunkai orogeny as the name of this event. Owing to the scarcity of synchronous intermediate-mafic rocks (e.g. Peng et al., 2006a; Wang et al., 2013b), details about the orogeny remain poorly defined, especially regarding the dynamic settings and the orogenic processes. A systematic geochronological, petrological, and geochemical investigation of the early Paleozoic granites will thus help to establish the temporal-spatial

evolution of the igneous activities in response to the thermal-chemical conditions during the orogeny.

Paleozoic granites are widespread in the eastern SCB (Fig. 1), occurring as laccoliths and batholiths, and are usually of large volume with a total exposure area of over 20,000 km². Some reliable ages and geochemical data for these granites have become available in recent years (e.g. Li et al., 2010; Shen et al., 2008; Wan et al., 2007, 2010; Wang et al., 2007, 2011, 2012; Xia et al., 2014; Xu et al., 2009; Zhang et al., 2009; Zhang et al., 2010, 2012; Zhao et al., 2013b). Geochronological studies have defined a wide age-span of ca. 381–462 Ma for these granites. Most of these granites are peraluminous S-type granites, with minor amphibole-bearing I-type granites, and they are thought to be petrogenetically related to the syn-orogenic to late-orogenic melting of the orogenically thickened crust (e.g. Li et al., 2010; Xia et al., 2014; Zhao et al., 2013b). Classification of the granites as I-type and S-type essentially depends on the nature of the source rocks, with the different types forming at the different stages of the orogeny. Thus, they do not provide unambiguous tectonic constraints on the orogenic processes (e.g. Clemens, 2003; Förster et al., 1997). Our recent work has led to recognition of two Devonian A-type granites in Central Jiangxi Province for the first time. The presence of A-type granites is particularly important because they may be indicative of a regional extensional tectonic environment and can thus be used to constrain the end of the syn-collisional compressional environment of the orogeny (e.g. Bonin, 2007; Eby, 1992; Loiselle and Wones, 1979; Turner et al., 1992; Whalen et al., 1987). Here, we present zircon U-Pb ages, mineral chemistry, major and trace element geochemistry, and Nd-Hf isotopic compositions of the two A-type granites and mafic microgranular enclaves in the granites. These results will be used to constrain their ages, petrogenesis and magma

sources, and thus provide direct constraints on the post-collisional extensional environment of the Wuyi–Yunkai orogeny.

2. Geological setting

The boundary between the Yangtze Block and the Cathaysia Block is marked by the northeasterly trending Jiangshan–Shaoxing Fault (Fig. 1), but the southwestern extension of this boundary is unclear due to poor exposure and multiple intense tectonic modifications. The SCB formed by amalgamation between the Yangtze and Cathaysia Blocks during the Neoproterozoic (e.g. Charvet, 2013; Li et al., 2009), and subsequently, a failed rift developed along the boundary and was filled with a thick sequence sediments that now comprise greywacke–slate–schist (e.g. Wang and Li, 2003). Later early-middle Paleozoic sequences are characterized by carbonate and siliciclastic rock successions.

The Wuyi–Yunkai orogeny was identified to be of early-middle Paleozoic age largely due to the recognition of an angular unconformity between post-Silurian cover and strongly deformed pre-Silurian strata (e.g. Huang, 1978; Ren, 1964, 1991; Ting, 1929). Contemporaneously, extensive metamorphism and granitic magmatism occurred in the southeastern half of South China Block (Fig. 1). The early-middle Paleozoic high-grade metamorphic rocks, which reach amphibolite to granulite facies, are mainly exposed in the Wuyi and Yunkai Mountains and have been studied in detail (e.g. Charvet et al., 2010; Chen and Zhuang, 1994; Li et al., 2010; Xu et al., 2011; Yu et al., 2003, 2005; Zhao and Cawood, 1999). In the eastern Wuyi–Yunkai orogeny, amphibolite-facies metamorphism occurred between ca. 460–440 Ma, followed by a phase of rapid unroofing from >8 kbar to ~4 kbar, possibly indicating thick-skinned NW-verging thrusting. The metamorphic

rocks cooled to below 300–500 °C by ca. 420 Ma (Li et al., 2010). In the southern Wuyi Domain, the Taoxi pelitic granulites have metamorphic ages of 445–479 Ma, a peak metamorphic pressure of 1.0–1.1 GPa and temperature of 835–878 °C (Yu et al., 2005). In the Yunkai Domain, garnet-bearing amphibolites occur within the gneiss and schist in the Yunkai Complex, reflecting metamorphic temperatures of 780–880 °C and pressure of 0.53–0.71 GPa (Yu et al., 2007).

The Paleozoic magmatic rocks in the eastern SCB are composed mainly of massive and gneissoid granites. Only a few contemporaneous basaltic rocks have been identified in the SCB (e.g. Peng et al., 2006a; Wang et al., 2013b). The gneissoid granites, or migmatites, are voluminous and mainly exposed along the Wuyi, Baiyun, Yunkai and Wugong domains (e.g. Li et al., 2010; Peng et al., 2006b; Wang et al., 2007, 2011). They show ductile deformation on their border, with gneissic to mylonitic fabrics (Charvet et al., 2010; Xu et al., 2011) suggesting a late tectonic emplacement, possibly synchronous with a general strike-slip environment (Charvet et al., 2010). The massive granitic rocks are widespread to the east of the Anhua–Luocheng fault in the eastern SCB and exhibit a planar-shaped pattern (e.g. Zhang et al., 2012).

3. Local geology

The Huitong and Epo granites are located in Central Jiangxi Province, South China, and they intruded into the Proterozoic–Devonian rocks (Fig. 2). The outcropping Pre-Cambrian basement rocks in Central Jiangxi are the Proterozoic Zhoutan Group, which consists mainly of schists, granulites and amphibolites. The protoliths of the schists and granulites were sedimentary, whereas the precursor to the amphibolites was basaltic origin (Hu and Zhang, 1998). The amphibolites yield a Sm–Nd

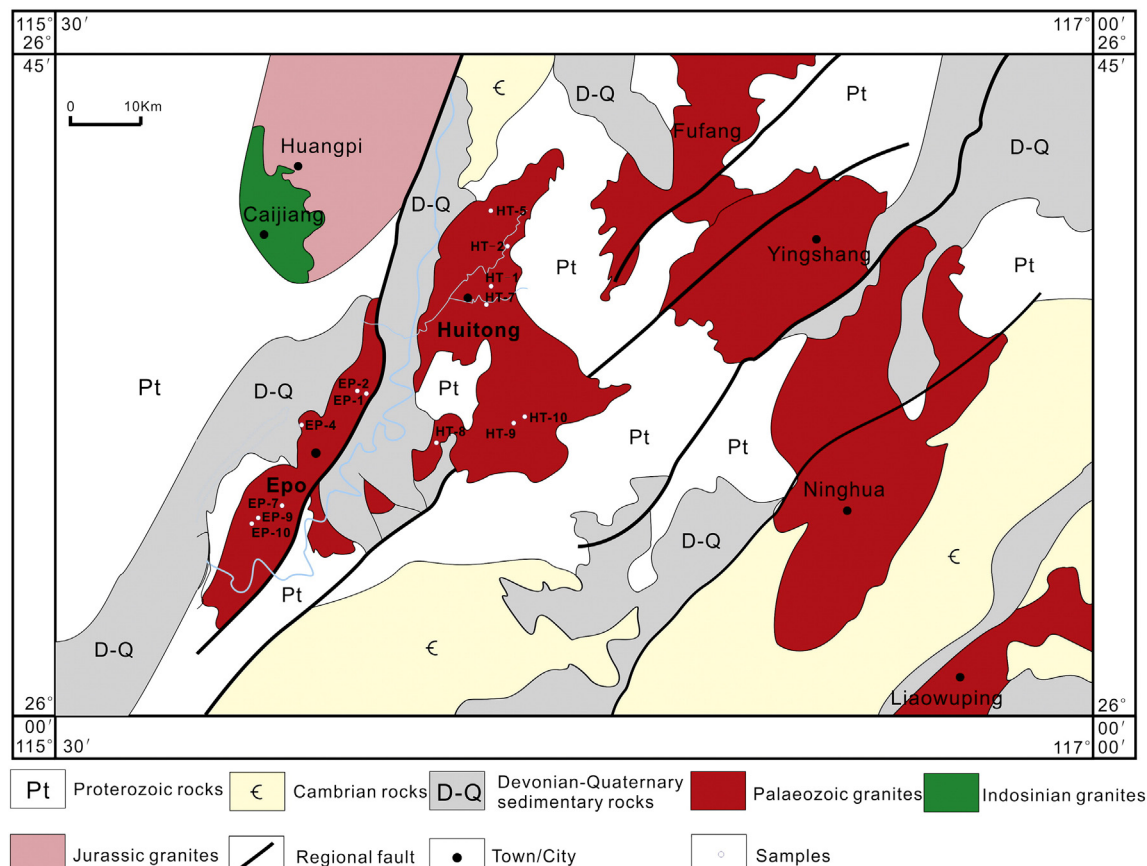


Fig. 2. Geological map of the Huitong and Epo plutons.

isochron age of 1113 ± 49 Ma ($\text{MSWD} = 0.22$) and a Palaeoproterozoic model age (2.4 Ga) (Hu et al., 1999). The parametamorphic rocks in Central Jiangxi Province show Meso- to Palaeoproterozoic Nd isotopic model ages (from 1.4 Ga to 2.1 Ga with an average value of 1.8 Ga, Hu and Zhang, 1999).

Some Paleozoic gneissoid and massive granites also occur in this area, including the gneissoid Fufang granite (434–444 Ma, Zhang et al., 2010), the massive Ninghua granite and Yingshang granite (ca. 451 Ma, Wang et al., 2011) (Fig. 2). These three granites have been classified as peraluminous S-type granites (Wang et al., 2011; Zhang et al., 2010). Later Indosian and Yanshanian granitic magmatism also occurred in this area, including intrusion of the Triassic A-type Caijiang granite (ca. 230 Ma, Zhao et al., 2013a), the Jurassic I-type Huangpi granite and S-type Daguzhai granite (ca. 154 Ma, Zhao et al., 2011).

4. Petrography

The Huitong granite forms a pluton with an outcrop area of about 350 km^2 and the Epo granite is located off the southwestern side of the Huitong granite with an outcrop area of about 200 km^2 (Fig. 2). Both granites are composed of mainly medium- to coarse-grained gray to pink porphyritic biotite monzogranites with porphyritic texture and massive structure (Fig. 3a, c). They also have similar mineral assemblages, with phenocrysts of $\sim 30 \text{ vol.\%}$ K-feldspar (with size ranging

from 2 to 5 cm) in a groundmass ($\sim 70 \text{ vol.\%}$) that consists of quartz (30 vol.\%), K-feldspar (25 vol.\%), plagioclase (35 vol.\%), and interstitial biotite (10 vol.\%). Biotite occurs as mineral aggregates along the boundary of coarse grained K-feldspar, plagioclase and quartz (Fig. 3b, d), indicating that biotite crystallized later than plagioclase and quartz. Accessory minerals include monazite, apatite, zircon, magnetite and ilmenite.

Circular or lenticular mafic microgranular enclaves (MMEs) are widespread in the Huitong and Epo granites (Fig. 3e, f), and appear are centimeters to decimeters in size. The MMEs are granodioritic-dioritic in composition and composed of biotite (20–30 vol.\%), plagioclase (20–30 vol.\%), K-feldspar (20–30 vol.\%) and quartz (20–30 vol.\%). Plagioclase occurs both as small euhedral laths and as larger mantled crystals. Biotite is typically subhedral and forms monomineralic clots with lobate outlines, or small anhedral crystals interstitial to plagioclase and quartz. Large K-feldspar crystals often crosscut the enclave/host boundary (Fig. 3e). This suggests that the large K-feldspar crystals within the enclaves are probably xenocrysts captured from the partially crystalline host magma by the enclave magma (e.g. Vernon et al., 1988; Perugini et al., 2003). Apatites in MMEs display euhedral acicular habits with crystals elongated along the “c” crystallographic axis (Fig. 3f), and are indicative of rapid cooling and crystallization (e.g. Sparks and Marshall, 1986).

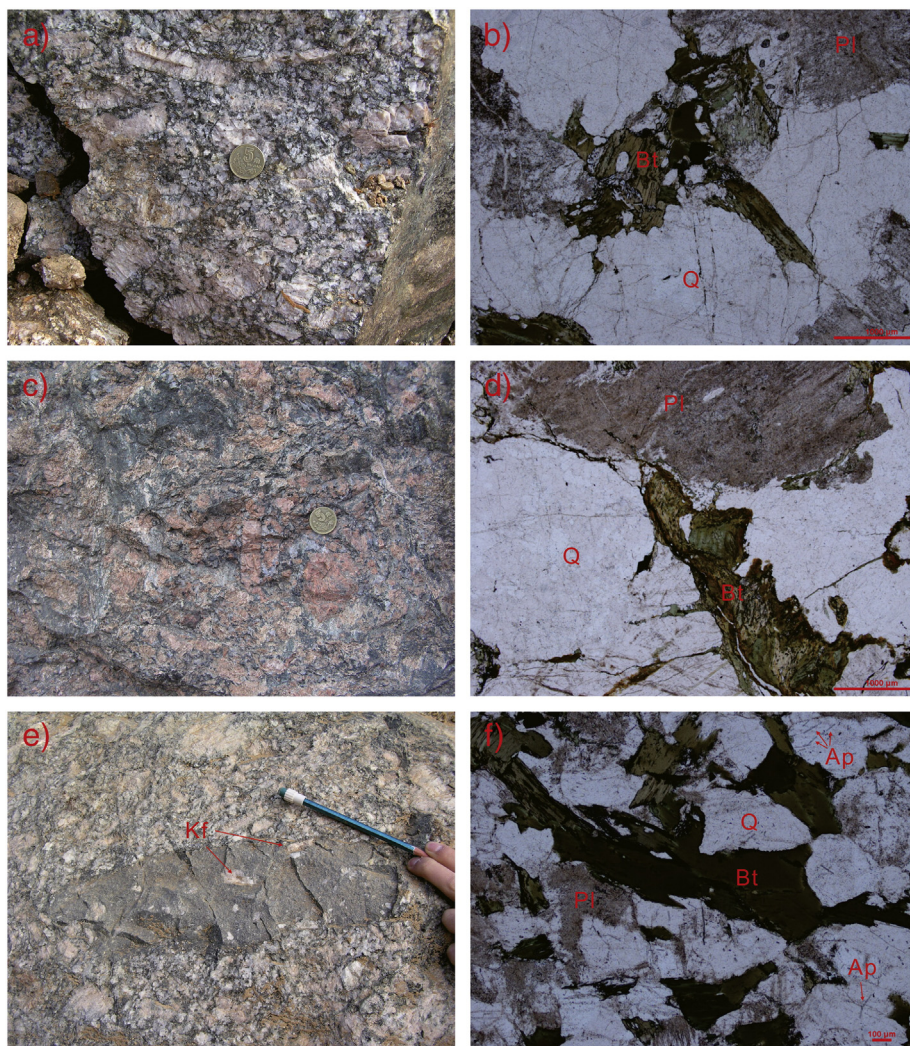


Fig. 3. Photographs of representative granite and MME samples from the Huitong and Epo plutons. (a)–(b), the Huitong granite; (c)–(d), the Epo granite; (e)–(f), the MMEs. Bt—biotite, Kf—K-feldspar, Pl—plagioclase, Q—quartz, Ap—apatite.

5. Analytical methods

5.1. Zircon U-Pb dating

Zircons were separated from three granite samples (HT-9a from the Huitong granite, EP-2a and EP-4 from the Epo granite) and one MME sample (HT-9b from a MME in the Huitong granite) by crushing, magnetic and heavy liquid separations, and then handpicked under a binocular microscope. The zircons were mounted in epoxy resin and then polished to approximately half their thickness before being examined under transmitted and reflected light, and cathodoluminescence (CL) to reveal their internal structures. CL images were obtained by using a MonoCL 3+ detector attached to a scanning electron microscope at the State Key Laboratory of Continental Dynamics, Northwest University.

In-situ zircon U-Pb isotopic analyses were undertaken using an Agilent 7500a ICP-MS equipped with a New Wave UP 213 nm laser-ablation system at the State Key Laboratory for Mineral Deposits Research, Nanjing University. Analyses were carried out with a beam diameter of 30 μm , 5 Hz repetition rate and laser energy of 12 J/cm². Helium was used as carrier gas to transport the ablated sample into the ICP-MS. Each run comprised 10–12 unknown sample analyses, bracketed by four GJ-1 and two Mud Tank zircon standards. The results were calculated using the GLITTER program (Van Achterbergh et al., 2001). The method of Andersen (2002) was adopted for the common Pb correction.

5.2. Mineral chemistry

Quantitative analyses of the minerals were carried out on polished thin sections using a JEOL JXA-8100 electron-microprobe (EMP) at the State Key Laboratory for Mineral Deposits Research at Nanjing University. The operating conditions included an accelerating voltage of 15 kV and a probe current of 2×10^{-8} A for most elements. The counting times at the peaks were 10 s for the major elements. The diameter of the electron beam was 1 μm . All data were corrected with standard ZAF correction procedures. The following standards were used for quantitative elemental analyses: hornblende (Na, K, Ca, Fe, Mg, Al, Si), MnTiO₃ (Mn, Ti) and topaz (F) for biotite, and hornblende (Na, K, Ca, Fe, Mg), fayalite (Si) and topaz (Al) for alkali feldspar and plagioclase.

5.3. Major and trace element contents of whole rock samples

Major element contents of whole rock samples were determined using an ARL-9800 XRF at the Modern Analysis Center of Nanjing University, with analytical uncertainties better than 0.5% for most elements. Trace element contents were determined by a Finnigan MAT Element II HR-ICP-MS at State Key Laboratory for Mineral Deposits Research, Nanjing University, using analytical procedures similar to those described by Gao et al. (2003). About 50 mg of powdered samples was dissolved in high pressure Teflon bombs using a HF + HNO₃ mixture. Rh was used as an internal standard to monitor signal drift during ICP-MS measurement. The USGS rock standards GSP-1, AGV-2 were chosen for calibrating element concentrations of the measured samples. Analytical uncertainties for most elements were typically lower than 5%.

5.4. Sr-Nd isotopic compositions of whole rock samples

Sr and Nd isotope analyses of whole rock samples were undertaken using the chemical separation and mass spectrometry methods described in Pu et al. (2004, 2005). About 100 mg samples were dissolved in the same way as for trace element analyses. Complete separation of Sr was achieved by a combination of cation-exchange chromatography in H⁺ form and pyridinium form with the DCTA complex. Nd was then separated from the REE fractions by cation-exchange resin using HIBA as eluent. Each separated Sr sample was dissolved in 1 μl 1 N HCl and

then loaded with TaF₅ solution onto a W single filament. Each purified Nd sample was dissolved in 1 μl 1 N HCl and then loaded with H₃PO₄ onto a Re double-filament. Determination of Sr and Nd isotopic compositions was carried out using a Finnigan MAT Triton TI TIMS at the State Key Laboratory for Mineral Deposits Research, Nanjing University. Sr isotopic data were normalized to ⁸⁶Sr/⁸⁸Sr = 0.1194 and Nd isotopic data were normalized to ¹⁴⁶Nd/¹⁴⁴Nd = 0.7219. During the analysis period for our samples, the NIST-987 Sr standard gave an average value of 0.710258 ± 0.000006 ($n = 10, 2\sigma$) and the JNDI-1 Nd standard gave an average value of 0.512118 ± 0.000005 ($n = 10, 2\sigma$), which is similar to the referenced value of 0.512115 ± 0.000007 (Tanaka et al., 2000). For the calculation of $\epsilon_{\text{Nd}}(t)$ values, we adopted a decay constant for ¹⁴⁷Sm of $6.54 \times 10^{-12} \text{ year}^{-1}$ (Lugmair and Marti, 1978) and chondritic values of ¹⁴³Nd/¹⁴⁴Nd (0.512638) and ¹⁴⁷Sm/¹⁴⁴Nd (0.1967) (Jacobsen and Wasserburg, 1980). Depleted mantle values of ¹⁴³Nd/¹⁴⁴Nd (0.513151), ¹⁴⁷Sm/¹⁴⁴Nd (0.2136) and a mean crustal value of ¹⁴⁷Sm/¹⁴⁴Nd (0.118) (Jahn and Condie, 1995) were used for calculating two-stage depleted mantle model ages.

5.5. Zircon Hf isotopes

In-situ zircon Hf isotope analyses were performed using a New Wave UP 193 nm laser ablation system attached to a Neptune Plus MC-ICP-MS at the State Key Laboratory for Mineral Deposits Research at Nanjing University. A stationary spot with a beam diameter of 35 μm was used for the analyses. Helium was used as a carrier gas to transport the ablated samples from the laser-ablation cell to the ICP-MS torch via a mixing chamber mixed with argon. For instrumental mass bias correction, the Yb isotope ratios were normalized to a ¹⁷²Yb/¹⁷³Yb ratio of 1.35274, and the Hf isotope ratios were normalized to a ¹⁷⁹Hf/¹⁷⁷Hf ratio of 0.7325 using an exponential law (Chu et al., 2002). The details of the mass bias correction protocols were the same as those described by Wu et al. (2006). Standard zircon GJ-1 (age: 608 Ma, Jackson et al., 2004) was used as the reference standard during the routine analyses, and yielded a weighted mean ¹⁷⁶Hf/¹⁷⁷Hf ratio of 0.282015 ± 0.000008 ($2\sigma, n = 37$), which is similar to the precision and accuracy of the solution analysis method of Morel et al. (2008). The decay constant of $1.865 \times 10^{-11} \text{ year}^{-1}$ for ¹⁷⁶Lu (Scherer et al., 2001) and the present-day chondritic values of ¹⁷⁶Lu/¹⁷⁷Hf (0.0332) and ¹⁷⁶Hf/¹⁷⁷Hf (0.282772) (Blichert-Toft and Albarède, 1997) were adopted to calculate the initial values of ¹⁷⁶Hf/¹⁷⁷Hf and $\epsilon_{\text{Hf}}(t)$. Depleted mantle Hf model ages (T_{DM}) were calculated from the measured ¹⁷⁶Lu/¹⁷⁷Hf and ¹⁷⁶Hf/¹⁷⁷Hf ratios of the zircons assuming a present-day ¹⁷⁶Hf/¹⁷⁷Hf ratio of 0.283250 and a ¹⁷⁶Lu/¹⁷⁷Hf ratio of 0.0384 for the depleted mantle (Griffin et al., 2002). The average crustal ¹⁷⁶Lu/¹⁷⁷Hf value of 0.015 was adopted to calculate the two-stage model ages (T_{DM}^c) (Griffin et al., 2002).

6. Results

6.1. Zircon U-Pb data

6.1.1. The Huitong granite

Sample HT-9a (location: N26°22'27.0", E116°09'2.9") is collected from the Huitong granite and is a fresh porphyritic biotite granite. Zircons from this sample are colorless, euhedral, elongate to stubby grains. Most zircon grains have a length of 200–300 μm and a width of 50–100 μm . Length/width ratios mostly vary from 2:1 to 4:1. In CL images, the zircons show well-developed oscillatory zoning, implying a magmatic origin (Hoskin and Schaltegger, 2003; Wu and Zheng, 2004).

The zircon U-Pb dates are listed in the Supplemental electronic data Table. Eighteen spot analyses on the rims of eighteen zircon grains from the Sample HT-09a were obtained. U contents vary from 288 to 2157 ppm, and Th contents vary from 50 to 3482 ppm. Th/U ratios vary from 0.08 to 3.58. One spot yielded a relatively younger age (400 Ma), that maybe caused by loss of radiogenic Pb. The remaining

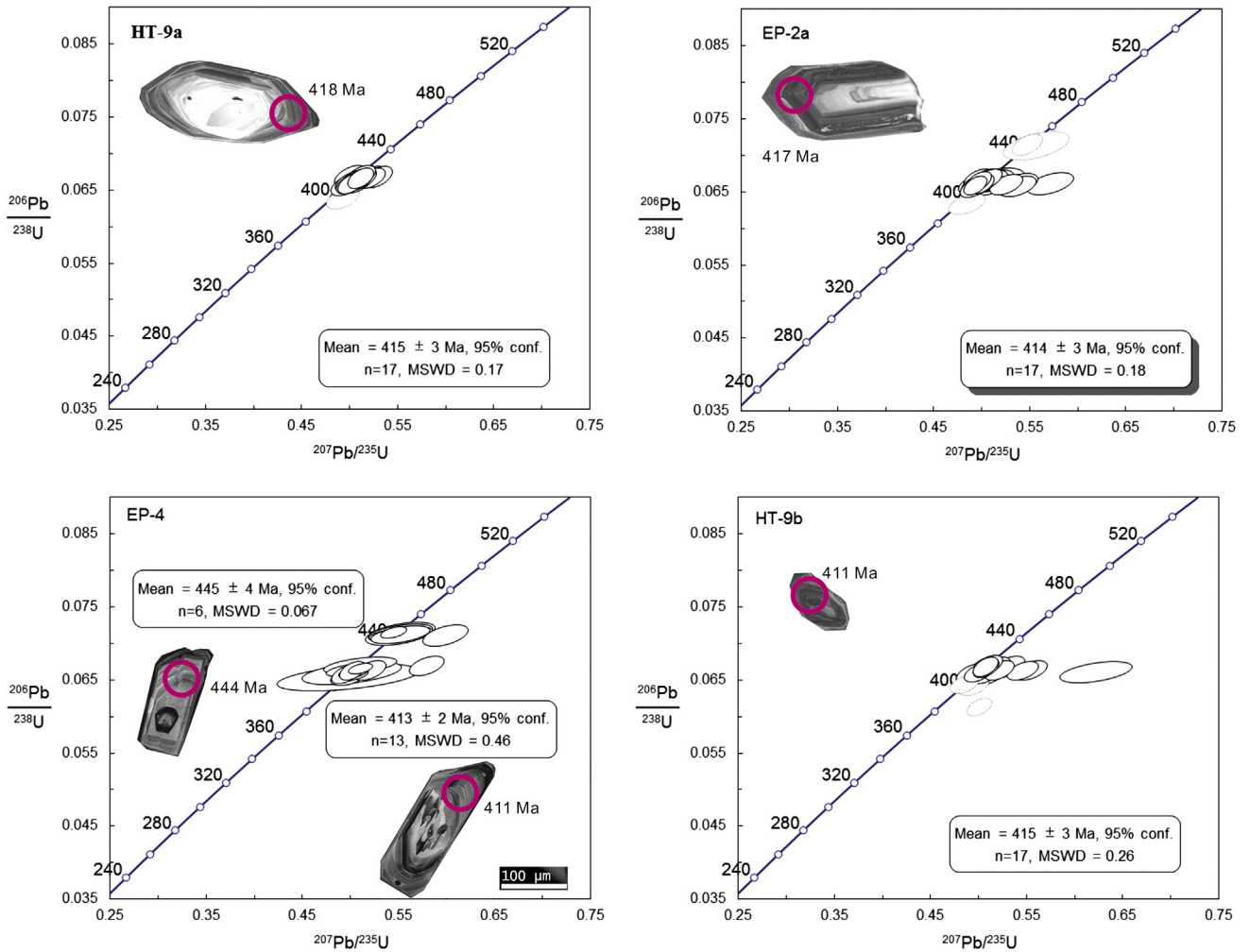


Fig. 4. LA-ICP-MS zircon U-Pb Concordia diagrams for the Huitong and Epo granites and the MMEs and representative zircon grains on analyzed spots with $^{206}\text{Pb}/^{238}\text{U}$ ages.

seventeen spot analyses gave similar $^{206}\text{Pb}/^{238}\text{U}$ ages varying from 410 Ma to 418 Ma, with a weighted average age of 415 ± 3 Ma ($n = 17$, $\text{MSWD} = 0.17$) (Fig. 4a). This average age is regarded as the emplacement age of the Huitong granite.

6.1.2. The Epo granite

Samples EP-2a (location: N26°24'55.5", E115°57'46.4") and EP-4 (location: N26°22'22.7", E115°56'56.3") were collected from the Epo granite. Both samples are of fresh porphyritic biotite granites. The zircons are euhedral and elongate. Most grains have lengths of 100–300 µm and widths of 50–100 µm. Length/width ratios mostly vary from 1:1 to 3:1. In CL images, the zircons show obvious oscillatory zoning that are typical of magmatic crystallization zircons.

Twenty spot analyses on twenty zircon grains were obtained from sample EP-2a. U contents vary from 75 to 946 ppm, and Th contents vary from 71 to 585 ppm. Th/U ratios vary from 0.18 to 2.18. One spot yielded a relatively younger age (396 Ma), and two spots yielded relatively older ages (444 Ma and 445 Ma). The remaining seventeen spots gave consistent $^{206}\text{Pb}/^{238}\text{U}$ ages of 410 to 417 Ma and yielded a weighted average age of 414 ± 3 Ma ($n = 17$, $\text{MSWD} = 0.18$) (Fig. 4b).

Twenty spot analyses on twenty zircon grains were obtained from sample EP-4. U contents of vary from 46 to 1413 ppm, and Th contents vary from 89 to 603 ppm. Th/U ratios vary from 0.23 to 2.08. One spot yielded a relatively old age (667 Ma), indicating an inherited source. Six spots yielded relatively consistent, but older ages (443 Ma to 446 Ma), giving a weighted average age of 445 ± 4 Ma ($n = 6$, $\text{MSWD} = 0.067$). The remaining thirteen spots gave consistent $^{206}\text{Pb}/^{238}\text{U}$ ages

of 408 to 418 Ma and yielded a weighted average age of 413 ± 2 Ma ($n = 13$, $\text{MSWD} = 0.46$) (Fig. 4c).

Thus, the emplacement age of the Epo granite is suggested to be 414 ± 3 Ma. It is therefore coeval with the Huitong granite, and both granites are considered to have formed from the same magmatic event.

6.1.3. The mafic microgranular enclaves

Sample HT-9b (location: N26°22'27.0", E116°09'2.9") was collected from a mafic microgranular enclave in the Huitong granite, and is a fresh thin-grained granodiorite. Zircons from the sample are smaller in size than those from the host granite (HT-9a). The zircons are euhedral with lengths of 50–100 µm and widths of 30–60 µm. The zircons also show obvious oscillatory zoning typical of magmatic crystallization (Fig. 4d).

Twenty spot analyses of twenty zircon grains from HT-9b were obtained. U contents vary from 186 to 940 ppm, and Th contents vary from 76 to 2338 ppm. Th/U ratios vary from 0.12 to 2.49. Three spots yielded a relatively younger age (384 Ma, 402 Ma and 403 Ma). The remaining seventeen spots gave consistent $^{206}\text{Pb}/^{238}\text{U}$ ages of 411 Ma to 419 Ma and yielded a weighted average age of 415 ± 3 Ma ($\text{MSWD} = 0.26$) (Fig. 4d). The age is consistent with that of the host Huitong granite.

6.2. Mineral chemistry

6.2.1. The Huitong granite

Representative electron microprobe analyses and chemical formulae calculated for biotite are listed in Table 1. Biotites from the Huitong

Table 1

Representative electron microprobe analyses and structural formula of biotites from the Huitong and Epo granites and the MMEs.

Samples	Huitong granite		Epo granite		MME
	HT-8	HT-9a	EP-7	EP-9	HT-9b
	n = 11	n = 12	n = 9	n = 10	n = 11
SiO ₂	34.55	33.25	35.14	35.24	35.56
TiO ₂	2.66	2.28	2.46	2.75	2.65
Al ₂ O ₃	18.76	17.39	18.08	18.83	17.75
FeO	24.37	27.55	26.65	22.30	23.57
MnO	0.37	0.39	0.41	0.38	0.30
MgO	6.43	5.96	5.52	7.19	8.08
CaO	0.03	0.02	0.07	0.01	0.05
Na ₂ O	0.10	0.19	0.08	0.09	0.14
K ₂ O	9.63	9.51	9.16	9.49	9.23
F	0.33	0.32	0.20	0.06	0.00
Total	97.07	96.62	97.67	96.28	97.32
Si	5.32	5.26	5.41	5.39	5.41
Al ^{IV}	2.68	2.74	2.59	2.61	2.59
Al ^{VI}	0.73	0.50	0.70	0.79	0.59
Ti	0.31	0.27	0.29	0.32	0.30
Mg	1.48	1.40	1.27	1.64	1.83
Fe	3.14	3.64	3.43	2.85	3.00
Mn	0.05	0.05	0.05	0.05	0.04
Ca	0.00	0.00	0.01	0.00	0.01
K	1.89	1.92	1.80	1.85	1.79
Na	0.03	0.06	0.02	0.03	0.04
F	0.16	0.16	0.10	0.03	0.03
OH*	3.84	3.84	3.90	3.97	3.97
Fe ²⁺ /(Fe ²⁺ + Mg ²⁺)	0.68	0.72	0.73	0.64	0.62

granite display high FeO contents (23.7%–28.0%) and medium MgO contents (5.4%–6.8%). They are close to the Fe-rich siderophyllite–annite end member, with high Fe²⁺/(Fe²⁺ + Mg²⁺) ratios between 0.67 and 0.74. The compositions of igneous biotites generally reflect the nature of their parental host magmas (e.g. Abdel-Rahman, 1994; Dahlquist et al., 2014), and the relatively high Fe²⁺/(Fe²⁺ + Mg²⁺) ratios in the biotite are typical of A-type granites (e.g. Dahlquist et al., 2010; 2014; Zhao et al., 2012).

Representative electron microprobe analyses for plagioclase and K-feldspar are listed in Table 2. Plagioclases from the Huitong granite are mainly oligoclase and andesine with Ab contents of 63%–77% and An contents of 22%–36%. K-feldspars display high contents of Or (92%–96%) and with minor amounts of Ab (0.04%–0.08%) and negligible An.

6.2.2. The Epo granite

The Epo granite has similar mineral chemistry to the Huitong granite. Biotites from the Epo granite have high FeO contents (23.2%–27.2%), medium MgO contents (5.3%–8.3%) and Fe²⁺/(Fe²⁺ + Mg²⁺) ratios of 0.60–0.74.

Plagioclases from the Epo granite are mainly oligoclase and andesine with Ab contents of 64%–79% and An contents of 21%–35%. K-feldspars display high contents of Or (90%–96%).

Table 2

Representative electron microprobe analyses and structural formula of plagioclases and K-feldspars from the Huitong and Epo granites and the MMEs.

Samples	Huitong granite		Epo granite		MME	
	Plagioclase (n = 7)	K-feldspar (n = 6)	Plagioclase (n = 7)	K-feldspar (n = 7)	Plagioclase (n = 10)	K-feldspar (n = 6)
Na ₂ O	6.53	0.60	7.33	0.74	8.24	0.32
Al ₂ O ₃	24.53	19.32	24.42	19.36	25.07	19.35
SiO ₂	63.70	64.49	63.08	63.93	60.34	63.81
K ₂ O	0.14	15.37	0.14	15.67	0.33	15.93
CaO	4.83	0.03	4.90	0.06	5.53	0.28
Total	99.78	99.87	99.94	99.80	99.61	99.82
An	0.29	0.00	0.27	0.00	0.26	0.01
Ab	0.70	0.06	0.72	0.07	0.72	0.03
Or	0.01	0.94	0.01	0.93	0.02	0.96

6.2.3. The mafic microgranular enclaves

Biotites from the MMEs have slightly lower FeO contents (22.6%–24.6%) and higher MgO contents (7.9%–8.3%) than those from the host granites. Fe²⁺/(Fe²⁺ + Mg²⁺) ratios vary from 0.61 to 0.63.

Plagioclases from the MMEs are mainly oligoclase and andesine with Ab contents of 68%–73% and An contents of 25%–31%. K-feldspars display high contents of Or (96%–99%).

6.3. Major element and trace element compositions

6.3.1. The Huitong granite

The major and trace element contents of the Huitong granite samples are listed in Table 3. The Huitong granite has variable SiO₂ contents of 67.23% to 73.96%, with an average of 70.72%. It has high Al₂O₃ (12.72–14.77%) and low CaO contents (0.14–1.85%). Total K₂O + Na₂O contents vary from 6.96%–9.39%. In the plot of SiO₂ vs. alkalinity ratios, all samples plot in the alkaline field (Fig. 5, Wright, 1969). The Huitong granite is peraluminous to strongly peraluminous, with A/CNK (molar ratio of Al₂O₃/(CaO + Na₂O + K₂O)) ratios ranging from 1.05 to 1.50. The granite has relatively high Fe₂O₃ content (2.09–4.07%), and low MgO (0.26–1.05%) and CaO contents (0.14–1.85%). FeO^T/MgO ratios vary from 3.46 to 9.26 with an average of 4.56, and are clearly higher than those of I-type (average 2.27 of 991 samples) and S-type granites (average 2.38 of 578 samples) (Whalen et al., 1987). P₂O₅ contents vary from 0.11 to 0.30%, decreasing with increasing SiO₂ contents (Fig. 6). Thus, the primary magma is of a metaluminous and/or alkaline character (Chappell, 1999; Li et al., 2007).

Most of the samples have high rare earth elements (REEs), with total REE concentrations of 170–311 ppm (average 233 ppm). Chondrite-normalized REE patterns of the Huitong granite (Fig. 7a) invariably show a relative enrichment of light rare earth elements (LREEs), with high (La/Yb)_N ratios (8.6–24.0) and negative Eu anomalies (Eu/Eu^{*} = 0.14–0.18). In the primitive mantle-normalized trace element spidergram (Fig. 8a), all the samples show characteristic negative anomalies in Ba, Sr, Eu and Ti, and positive anomalies of Th, La, Nd, and Ce, that suggest a continental crust affinity. The Huitong granite is characterized by high contents of high field strength elements (HFSE), such as Zr (205–332 ppm), Y (22.1–39.7 ppm) and Nb (18.6–29.2 ppm). Total Zr + Nb + Ce + Y contents vary from 324 to 515 ppm. The granite also has high Ga/Al ratios, with 10,000 × Ga/Al values ranging from 2.73 to 3.44, which is similar to A-type granites of >2.6 (Whalen et al., 1987). In the discrimination diagrams of 10,000 × Ga/Al vs. Zr + Nb + Ce + Y and 10,000 × Ga/Al vs. K₂O + Na₂O (Fig. 9), all the samples fall in the field of A-type granites, and are distinct from most Paleozoic granites in South China.

6.3.2. The Epo granite

The Epo granite samples have similar geochemical characteristics to the Huitong granite. SiO₂ contents vary from 66.94 to 71.00%, and the

Table 3

Major element (in %) and trace element (in ppm) concentrations of the Huitong and Epo granites and the MMEs.

Element	Huitong granite							Epo granite						MME
	HT-1	HT-2	HT-5	HT-7	HT-8	HT-9a	HT-10	EP-1	EP-2a	EP-4	EP-7	EP-9	EP-10	HT-9b
SiO ₂	73.96	71.75	70.70	71.76	70.70	67.23	68.92	66.96	66.94	69.89	71.00	69.80	71.00	64.13
TiO ₂	0.28	0.37	0.34	0.27	0.54	0.71	0.65	0.59	0.44	0.47	0.38	0.45	0.42	1.22
Al ₂ O ₃	12.72	14.12	14.62	14.48	14.34	14.77	14.27	16.09	16.37	12.97	14.35	14.45	14.40	14.79
Fe ₂ O ₃	1.53	1.76	2.47	0.66	2.74	2.17	1.87	3.57	3.16	3.10	2.68	3.13	2.83	6.92
MnO	0.03	0.05	0.04	0.04	0.05	0.08	0.07	0.06	0.05	0.06	0.05	0.05	0.04	0.12
MgO	0.26	0.51	0.59	0.36	0.79	1.05	0.99	0.81	0.74	0.88	0.48	0.60	0.48	2.03
CaO	0.14	0.24	0.24	0.25	0.84	1.85	1.15	0.16	1.66	2.33	1.04	1.54	0.47	3.12
Na ₂ O	1.64	2.51	2.45	3.01	2.75	2.95	2.75	2.34	4.04	3.22	2.98	2.98	2.59	3.50
K ₂ O	5.94	4.45	6.48	6.38	5.34	5.33	4.77	5.64	4.81	4.56	5.66	5.50	5.95	2.48
P ₂ O ₅	0.11	0.16	0.11	0.14	0.25	0.26	0.30	0.18	0.20	0.20	0.18	0.20	0.11	0.38
LOI	2.00	2.69	1.68	1.19	1.23	1.42	1.87	3.63	1.68	2.06	0.61	0.61	1.14	1.21
Total	99.83	99.89	99.92	99.97	99.89	99.68	99.81	100.03	100.11	99.74	99.57	99.51	99.59	99.89
KN/A	0.72	0.63	0.76	0.82	0.72	0.68	0.62	0.73	0.79	0.77	0.75	0.74	0.57	
A/CNK	1.35	1.5	1.27	1.17	1.21	1.05	1.21	1.57	1.1	0.89	1.11	1.06	1.24	1.05
FeO ^T /MgO	9.26	5.38	4.14	5.3	3.49	3.46	3.69	3.96	3.83	3.19	5.03	4.70	5.31	3.07
K ₂ O + Na ₂ O	7.58	6.96	8.93	9.39	8.09	8.28	7.52	7.98	8.85	7.78	8.64	8.48	8.54	5.98
Al ₂ O ₃ /TiO ₂	45.4	38.2	43.0	53.6	26.6	20.8	22.0	27.3	37.2	27.6	37.8	32.1	34.3	12.1
A.R.	3.87	2.88	4.01	4.52	3.28	2.99	2.90	2.93	2.93	3.07	3.56	3.26	3.70	2.00
Li	38.76	76.59	44.52	34.69	149.22	55.07	67.96	33.54	33.06	65.7	75.87	69.79	63.77	106.6
Be	2.41	5.69	2.18	5.00	3.94	3.37	4.77	2.30	3.88	1.97	3.06	2.12	2.94	4.04
Sc	4.35	12.3	5.89	4.61	6.70	9.82	10.2	9.02	6.34	6.94	4.98	6.05	5.42	17.1
Ti	1725	2286	2144	1637	3031	4568	4358	3559	2730	3269	2284	2964	2568	8247
V	21.06	30.60	27.23	19.51	44.89	65.10	60.38	38.74	29.19	38.83	20.85	25.88	22.73	139.2
Cr	1404	1095	1823	802.2	1534	1230	429.6	17.68	21.45	107.9	23.29	59.86	24.27	3168
Mn	281.0	483.7	388.7	351.5	432.9	695.8	608.3	368.0	364.5	376.8	554.0	634.0	485.0	1266
Co	10.6	9.49	12.7	6.49	12.7	14.4	10.1	6.66	5.59	6.82	4.48	5.97	6.25	30.6
Ni	971.9	629.2	1178	523.7	1009	794.4	275.4	1.98	5.37	73.3	3.07	5.12	4.98	1923
Cu	18.61	15.68	21.82	11.24	21.39	22.33	10.73	4.33	3.97	13.32	6.86	9.67	5.46	50.13
Zn	144.4	165.5	536.7	117.5	404.6	145.0	113.0	164.1	107.2	56.68	59.46	59.08	64.85	237.4
Ga	20.41	22.05	21.6	20.95	21.35	23.33	25.98	21.70	21.67	19.61	21.21	20.96	20.62	28.84
Rb	320.0	262.0	260.0	295.0	292.0	227.0	245.0	129.7	215.4	170.0	263.0	220.0	274.0	248.9
Sr	74.61	119.39	116.44	78.81	92.12	195.2	192.6	135.0	220.8	144.6	117.0	137.0	120.0	162.0
Y	26.62	39.67	24.46	29.35	22.06	28.45	25.59	24.47	29.76	28.87	29.30	36.75	26.48	42.53
Zr	211.1	235.7	272.4	204.9	264.6	319.8	332.1	437.0	264.9	296.9	181.0	260.0	209.0	468.3
Nb	24.50	23.61	21.67	18.61	25.51	28.15	29.21	23.71	19.03	25.56	29.22	30.26	29.54	45.29
Mo	154.9	111.5	188.2	82.91	167.9	131.9	40.99	3.29	3.64	11.39	0.72	2.15	0.62	323.6
Cd	0.51	0.68	0.65	0.38	0.55	0.46	0.39	0.29	0.15	0.16	0.00	0.00	0.00	0.98
Sn	6.43	15.43	4.54	6.06	9.83	7.06	7.92	1.49	3.53	3.4	5.17	3.37	4.68	12.9
Cs	4.76	7.92	3.89	4.96	14.22	6.38	9.58	1.59	4.26	3.41	11.60	12.38	7.66	14.2
Ba	601.0	653.0	976.0	633.0	585.0	941.0	693.0	1826	696.0	650.0	766.0	794.0	906.0	193.0
Hf	5.82	7.45	6.64	5.16	6.21	7.65	7.4	11.8	7.09	8.27	5.47	7.45	6.07	10.5
Ta	2.15	2.56	1.52	1.8	2.16	2.05	2.76	1.31	1.61	1.75	1.63	1.28	1.57	2.48
W	7.44	9.28	9.58	4.2	7.46	5.74	2.58	0.97	0.69	1.56	2.17	1.54	1.64	10.2
Bi	0.36	0.51	0.17	0.25	0.38	0.21	0.22	0.12	0.23	0.13	0.23	0.19	0.26	0.30
Th	17.97	28.20	21.80	16.86	20.93	22.30	21.53	11.56	24.66	15.42	36.38	32.75	30.51	22.11
U	3.53	5.19	3.46	3.46	3.37	3.87	3.07	1.09	2.45	2.66	3.17	1.99	3.25	1.69
La	63.47	70.93	60.9	35.5	46.15	65.9	66.02	47.35	59.87	33.62	59.55	64.82	56.76	75.86
Ce	77.04	119.83	101.1	71.27	97.61	130.8	128.5	69.65	112.7	60.94	119.4	127.9	112.7	154.2
Pr	13.71	14.17	13.23	8.26	11.32	14.46	14.38	10.73	13.43	7.28	13.78	14.64	12.68	17.02
Nd	48.69	57.82	48.10	29.20	42.79	54.09	54.9	40.01	50.08	28.31	50.80	54.49	46.68	63.30
Sm	8.61	10.96	8.61	5.61	8.00	9.71	9.01	7.71	8.62	5.73	9.42	9.87	8.32	12.1
Eu	1.24	1.72	1.39	0.84	1.04	1.57	1.31	1.79	1.46	1.16	1.13	1.43	1.32	1.27
Gd	7.22	10.78	7.76	5.24	6.65	8.14	8.07	6.97	7.23	5.86	8.37	8.99	7.51	11.4
Tb	0.94	1.28	0.85	0.81	0.74	0.93	0.84	1.04	1.14	0.88	1.19	1.31	1.06	1.31
Dy	5.78	8.81	5.23	5.41	4.65	5.78	5.03	5.85	5.57	5.49	6.13	7.16	5.58	8.34
Ho	1.13	2.21	1.07	1.23	0.91	1.18	1.03	1.06	1.12	1.15	1.11	1.40	1.03	1.71
Er	3.00	6.39	3.02	3.41	2.47	3.04	2.85	3.05	3.22	3.05	3.29	4.32	3.11	4.64
Tm	0.43	0.80	0.38	0.47	0.32	0.41	0.32	0.41	0.42	0.32	0.46	0.63	0.44	0.57
Yb	2.56	5.59	2.37	2.71	1.95	2.07	1.85	2.77	2.89	1.44	2.99	4.01	2.88	3.29
Lu	0.36	0.79	0.36	0.37	0.30	0.30	0.25	0.40	0.39	0.22	0.45	0.60	0.43	0.49
ΣREE	234.0	312.0	254.0	170.0	225.0	298.0	294.0	198.0	268.0	155.0	278.1	301.6	260.5	355.0
(La/Yb) _N	16.69	8.55	17.32	8.82	15.96	21.48	24.01	11.51	13.95	15.74	13.46	10.92	13.32	15.54
(La/Sm) _N	4.64	4.07	4.45	3.98	3.63	4.27	4.61	3.86	4.37	3.69	3.98	4.13	4.29	3.96
(Gd/Yb) _N	2.27	1.56	2.64	1.56	2.75	3.18	3.51	2.03	2.02	3.28	2.32	1.85	2.17	2.79
δEu	0.16	0.16	0.17	0.15	0.14	0.18	0.15	0.24	0.19	0.2	0.39	0.46	0.51	0.11
10,000 × Ga/Al	3.03	2.95	2.79	2.73	2.81	2.98	3.44	2.55	2.50	2.86	2.79	2.74	2.70	3.68
Zr + Nb + Ce + Y	339.2	418.8	419.6	324.1	409.7	507.3	515.3	554.8	426.4	412.3	358.9	454.9	377.7	710.3
T _{zr}	841	858	854.0	820	847	845	868	920	829	822	802	829	827	876

alkalis are high (K₂O + Na₂O ranging from 7.78 to 8.85%). FeO^T/MgO ratios vary from 3.19 to 5.31 with an average of 4.33. The Epo granite also shows a peraluminous character, with A/CNK values (1.06–1.57) except one sample. P₂O₅ contents vary from 0.11% to 0.20%.

Total REE contents vary from 155 ppm to 302 ppm. Chondrite-normalized REE patterns of the Epo granite (Fig. 7b) are similar to those of the Huitong granite, with an enrichment of light rare earth elements (LREEs), high (La/Yb)_N ratios (10.9–15.7) and negative Eu

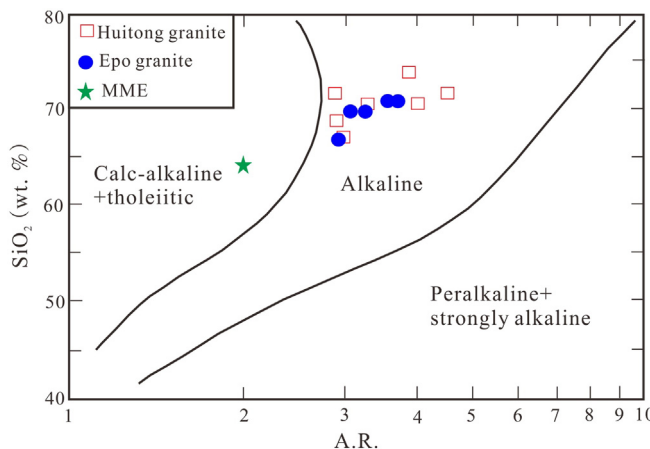


Fig. 5. A.R. vs. SiO_2 diagram for the Huitong and Epo granites and the MMEs, where A.R. (alkalinity ratio) = $[\text{Al}_2\text{O}_3 + \text{CaO} + (\text{Na}_2\text{O} + \text{K}_2\text{O})] / [\text{Al}_2\text{O}_3 + \text{CaO} - (\text{Na}_2\text{O} + \text{K}_2\text{O})]$ (wt.%).

anomalies ($\text{Eu}/\text{Eu}^* = 0.19\text{--}0.51$). In the primitive mantle-normalized spidergram (Fig. 8b), the samples are characterized by negative anomalies in Ba, Sr, Eu and Ti. The Epo granite also has high contents of HFSE, such as Zr (181–437 ppm), Y (24.5–36.8 ppm) and Nb (19.0–30.3 ppm). Total Zr + Nb + Ce + Y contents vary from 359 to 555 ppm. The granite also has high Ga/Al ratios, with $10,000 \times \text{Ga}/\text{Al}$ values ranging from 2.50 to 2.86. In the discrimination diagrams of $10,000 \times \text{Ga}/\text{Al}$ vs. Zr + Nb + Ce + Y and $10,000 \times \text{Ga}/\text{Al}$ vs. $\text{K}_2\text{O} + \text{Na}_2\text{O}$ (Fig. 9), all the samples fall in the field of A-type granites.

6.3.3. The mafic microgranular enclaves

One sample from the mafic microgranular enclaves in the Huitong granite has a SiO_2 content of 64.10%. It has higher total Fe_2O_3 (6.92%), MgO (2.03%), CaO (3.12%) and TiO_2 (1.22%) contents than the host granite, but a lower K_2O content (2.48%). The $\text{FeO}^\text{T}/\text{MgO}$ ratio is 3.07, which is lower than the host granite.

The MME sample has higher Sc, V, Cr, Ni and Mo contents than the host granite. It also has higher HFSE and REE contents (total REE = 355 ppm). The chondrite-normalized REE pattern for the enclave is marked by an enrichment in the LREEs and a negative Eu anomaly (Fig. 7c). In the primitive mantle-normalized spidergram (Fig. 8c), the sample is characterized by negative anomalies in Ba, Sr, Eu and Ti.

6.4. Isotopic results

6.4.1. The Huitong granite

The Sr–Nd isotopic compositions of the Huitong granite, the Epo granite and MME samples are presented in Table 4. The initial $^{87}\text{Sr}/^{86}\text{Sr}$ ratios and $\varepsilon_{\text{Nd}}(t)$ values have been calculated at 415 Ma. The Huitong samples have high $^{87}\text{Rb}/^{86}\text{Sr}$ ratios (2.78–12.5) that result in large uncertainties in the calculated $(^{87}\text{Sr}/^{86}\text{Sr})_i$ ratios. Hence, source discussions for these samples are mainly based on whole rock Nd and zircon Hf isotopic compositions. The Huitong granite samples have $^{147}\text{Sm}/^{144}\text{Nd}$ ratios of 0.099–0.116 and $^{143}\text{Nd}/^{144}\text{Nd}$ ratios of 0.511880–0.511963. Calculated $\varepsilon_{\text{Nd}}(t)$ values vary from –10.4 to –8.4 and two-stage model ages vary from 1.84 Ga to 2.00 Ga.

The in-situ Hf isotope analyses are listed in Table 5. $^{206}\text{Pb}/^{238}\text{U}$ ages of the zircon grains were used to calculate the initial $^{176}\text{Hf}/^{177}\text{Hf}$ ratios and $\varepsilon_{\text{Hf}}(t)$ values. The zircon average age (415 Ma) was used for those zircon grains without U–Pb ages. Twenty-four spots from sample HT-9a were obtained from the zircons, yielding initial $^{176}\text{Hf}/^{177}\text{Hf}$ ratios of 0.282108 to 0.282361, and $\varepsilon_{\text{Hf}}(t)$ values of –14.9 to –6.0. Most of $\varepsilon_{\text{Hf}}(t)$ values fall in the range of –9.0 to –5.0 (Fig. 10a). Two-stage Hf

model ages vary mostly from 1.80 Ga to 2.00 Ga (Fig. 10b), and are similar to the Nd isotopic model ages.

6.4.2. The Epo granite

The Epo granite samples have similar $\varepsilon_{\text{Nd}}(t)$ values to the Huitong granite, varying from –8.4 to –7.7. Two-stage model ages vary from 1.78 to 1.84 Ga. A total of eighteen spots on zircons from sample EP-4 were analyzed for Hf isotopic compositions, and the $\varepsilon_{\text{Hf}}(t)$ values vary from –10.5 to –3.9, and most of them fall in the range of –9.0 to –4.0 (Fig. 10c). The two-stage Hf isotopic model ages vary mostly from 1.70 to 2.00 Ga (Fig. 10d).

6.4.3. The mafic microgranular enclaves

The $\varepsilon_{\text{Nd}}(t)$ value of the MME sample in Huitong granite is –7.3, higher than the host Huitong granite. Two-stage model age for the MME sample is 1.75 Ga. A total of 12 spots on zircons from sample HT-9b were analyzed for Hf isotopic compositions. The $\varepsilon_{\text{Hf}}(t)$ values mostly vary from –11.5 to –3.5 (Fig. 10e). The two-stage Hf isotopic model ages vary mostly from 1.62 to 2.12 Ga (Fig. 10f).

7. Discussions

7.1. Petrogenetic type: A-type affinity

Since the introduction of the terms I- and S-type granites by Chappell and White (1974) and A-type granites by Loiselle and Wones (1979), granitic rocks have commonly been divided into these three types according to the nature of their protolith and their petrographical and geochemical features. The A-type granite classification was introduced to distinguish a group of granitic rocks, where A stands for alkaline, anorogenic and anhydrous (Loiselle and Wones, 1979). The presence of A-type granites has important tectonic implications, because they only occur in extensional tectonic environments, i.e., rift zones, anorogenic settings or post-collisional extensional settings (Eby, 1992). The scope of the definition of A-type granites has been expanded during the last decades (Bonin, 2007), but A-type granites still share some common petrographic and geochemical characteristics. Strict identification of A-type granite is thus important for using them for tectonic interpretations.

A-type granites are generally considered to be derived from relatively anhydrous and high-temperature magmas (Bonin, 2007; Loiselle and Wones, 1979), while I-type and S-type granites are derived from water-rich and low-temperature magmas (Clemens, 2003; Jung and Pfänder, 2007). For the Huitong and Epo granites, biotites occur along the boundary of euhedral plagioclase and quartz, which implies that biotite formed later than plagioclase and quartz (Fig. 3b, d). This interstitial biotite texture implies that the primary magma was relatively anhydrous. Zircon saturation thermometry (T_{Zr}) provides a simple and robust means to estimate the magma temperature of granites (Watson and Harrison, 1983). Miller et al. (2003) pointed out that zircon saturation temperatures calculated from bulk-rock compositions provide minimum estimates of magma temperature if the magma was undersaturated in Zr, but maxima if it was saturated. Although the Huitong and Epo granites have relatively high Zr contents (205–437 ppm), the two granites were likely undersaturated in Zr, based on the scarcity of restitic and inherited zircons. Thus, the calculated T_{Zr} from whole-rock compositions is likely to be a minimum estimate of their initial magma temperature. The calculated T_{Zr} of the Huitong granite is in the range of 820–868 °C using the equation of Watson and Harrison (1983). The calculated T_{Zr} of the Epo granite is in the range of 802–920 °C. The $\text{Al}_2\text{O}_3/\text{TiO}_2$ ratios of pelite- and psammite-derived melts are thought to be a function of T (Jung and Pfänder, 2007), so the relatively low $\text{Al}_2\text{O}_3/\text{TiO}_2$ ratios (20.8 to 53.6) for the Huitong and Epo granites indicate that their sources were partially melted under high temperature conditions (931–1006 °C). The estimated magma temperatures for the two granites

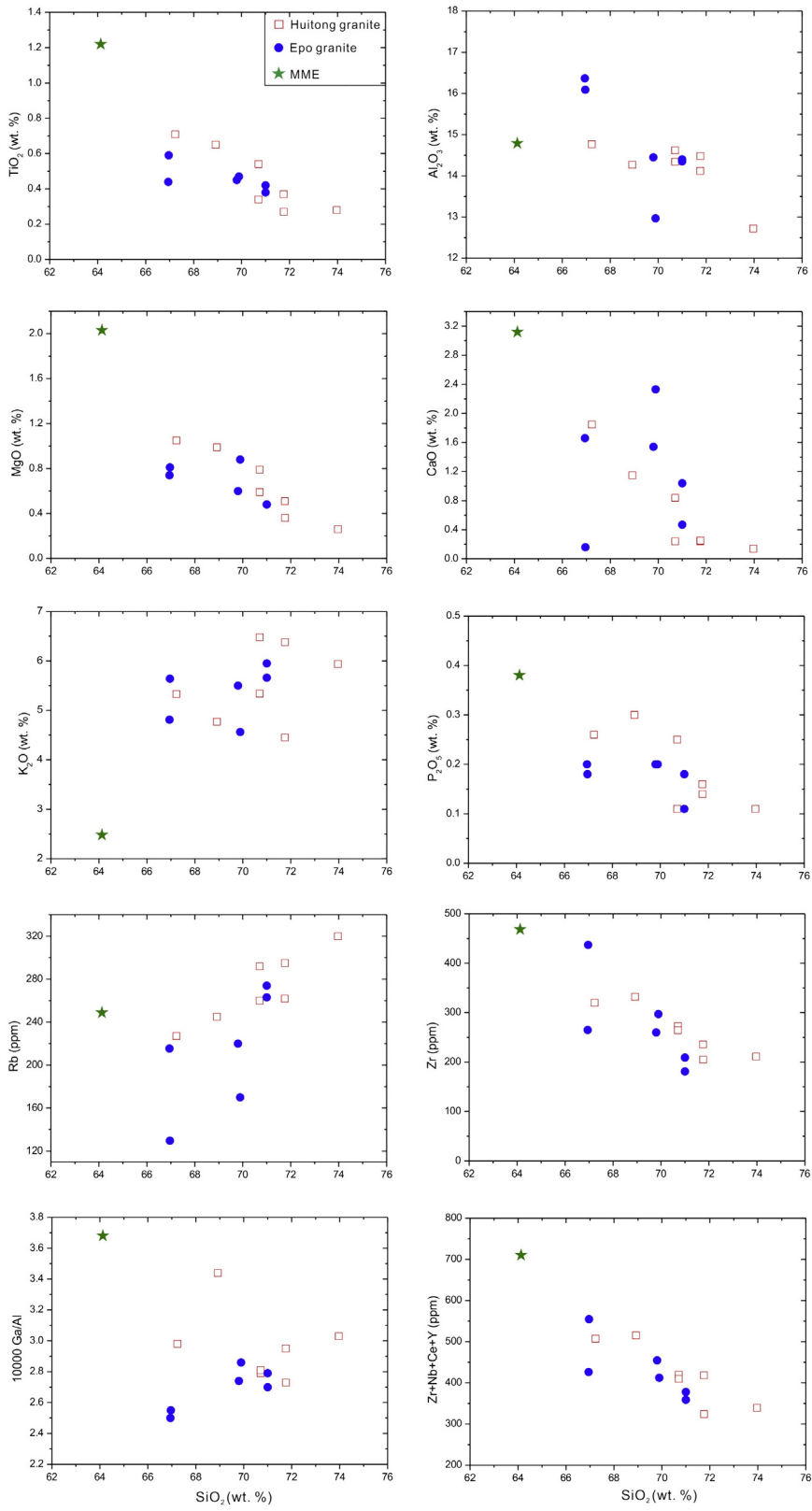


Fig. 6. Plots of selected major oxides (wt.%) and trace elements (ppm) vs. SiO₂ (wt.%) for the Huitong and Epo granites and the MMEs.

are similar to those for many other A-type granites (e.g. Dahlquist et al., 2014; King et al., 2001; Yang et al., 2012; Zhao et al., 2012, 2013a), but higher than those of common I-type granites and S-type granites (usually lower than 800 °C, e.g. King et al., 1997; Jiang et al., 2009). The relatively high melting and magma temperatures of the

Huitong and Epo granites suggest that they were derived from a refractory or dry source.

A-type granites share some common geochemical characteristics. They generally have high alkali metal contents, high HFSE contents (generally, Zr + Nb + Ce + Y > 350 ppm), high Ga/Al ratios (10,000 ×

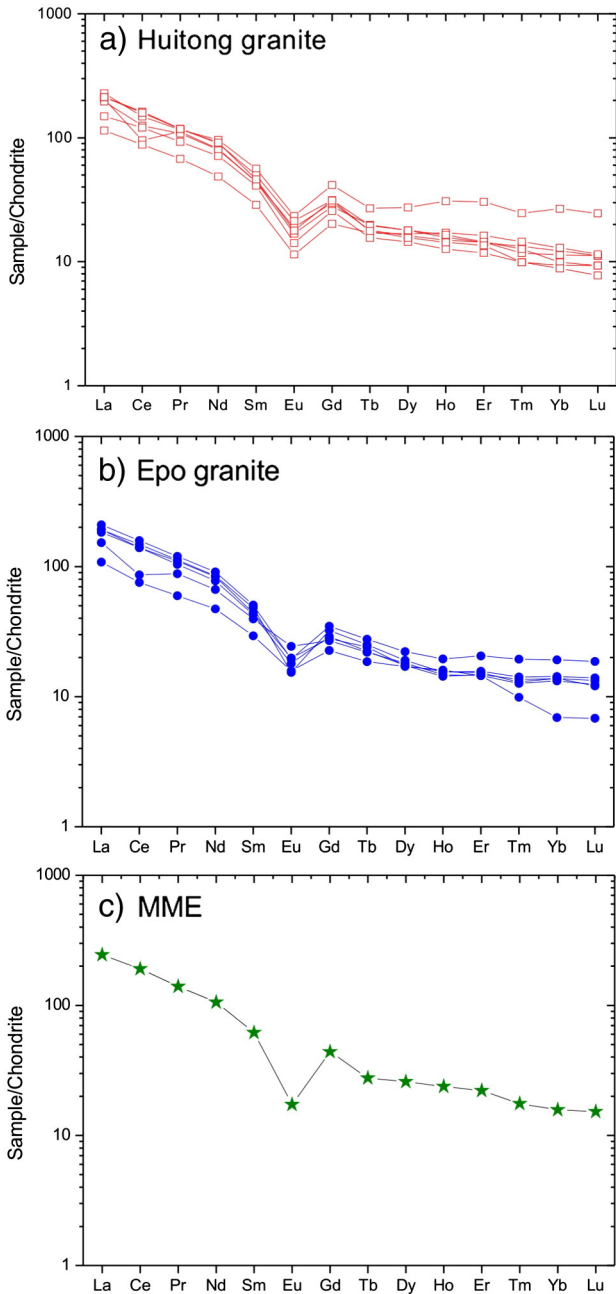


Fig. 7. Chondrite-normalized rare earth element diagrams for the Huitong and Epo granites and the MMEs. The normalization values of chondrite are from Boynton (1984).

$Ga/Al > 2.6$) and high total REE contents compared to I-type and S-type granites (Whalen et al., 1987). They also have high FeO^T/MgO ratios (King et al., 2001). Both the Huitong and Epo granites thus have A-type geochemical characteristics: high total alkali contents ($Na_2O + K_2O = 6.96\text{--}9.39\%$), high contents of HFSE ($Zr + Nb + Ce + Y = 324\text{--}555$ ppm), high $10,000 \times Ga/Al$ ratios (2.50–3.44), and high REE contents. In the $Zr + Nb + Ce + Y$ vs. $10,000 \times Ga/Al$ diagram (Whalen et al., 1987), the two granites plot in the A-type field (Fig. 9). These geochemical characteristics are clearly distinct from Paleozoic S-type and I-type granites in South China (eg. Wang et al., 2007, 2011; Shen et al., 2008; Zhang et al., 2009; Zhang et al., 2010, 2012; Zhao et al., 2013a). While highly fractionated S- and I-type granites have similarly high Ga/Al ratios to A-type granites (He et al., 2010a), the Ga/Al ratios here do not increase with increasing of SiO_2 contents (Fig. 6), suggesting the high Ga/Al ratios are a primary feature.

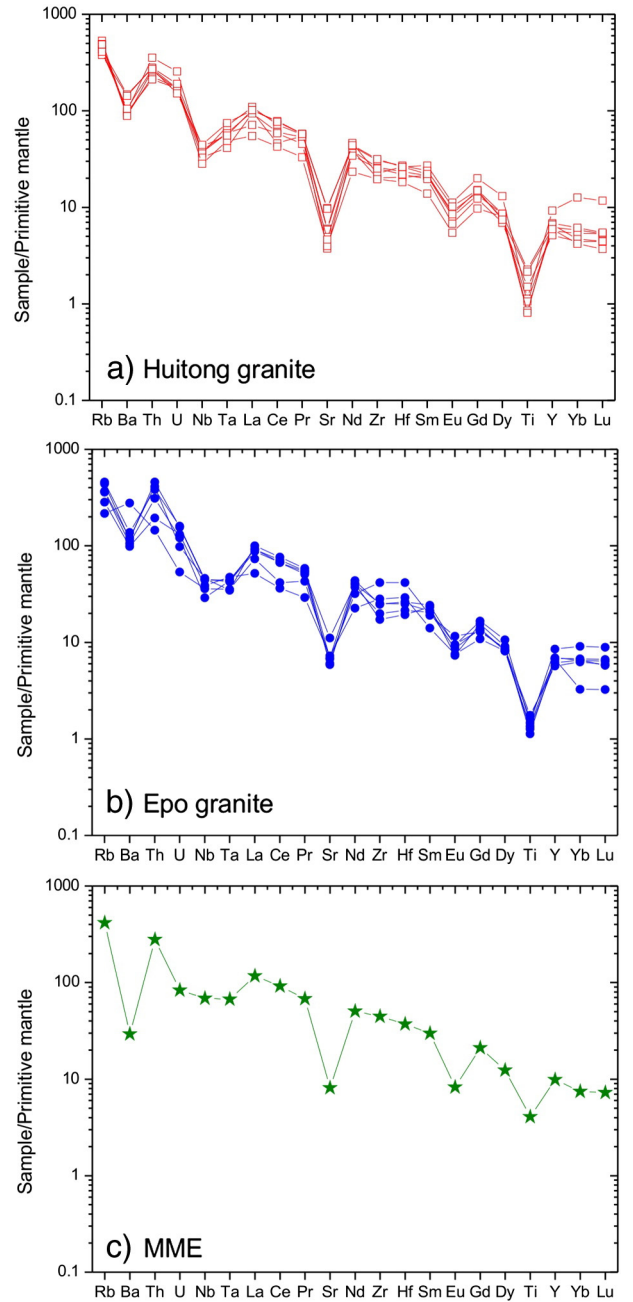


Fig. 8. Primitive mantle-normalized trace element spidergrams for the Huitong and Epo granites and the MMEs. The normalization values of chondrite are from Sun and McDonough (1989).

Granites containing both high Ga/Al ratios ($10,000 \times Ga/Al > 2.6$) and high HFSE contents ($Zr + Nb + Ce + Y > 350$ ppm) should belong to A-type (e.g. Wu et al., 2007).

7.2. Sources and petrogenesis

Many compositional variations have been found for A-type granites, and there is no consensus on their origin (Bonin, 2007). A-type granites are genetically diverse and can be produced from various sources and by different processes, hence several petrogenetic models have been proposed for their origin: (1) direct fractionation products of mantle-derived alkaline basalts (e.g. Litvinovsky et al., 2002; Mushkin et al., 2003; Turner et al., 1992); (2) partial melting of dry, lower crustal granulitic residue from which a granitoid melt was previously extracted

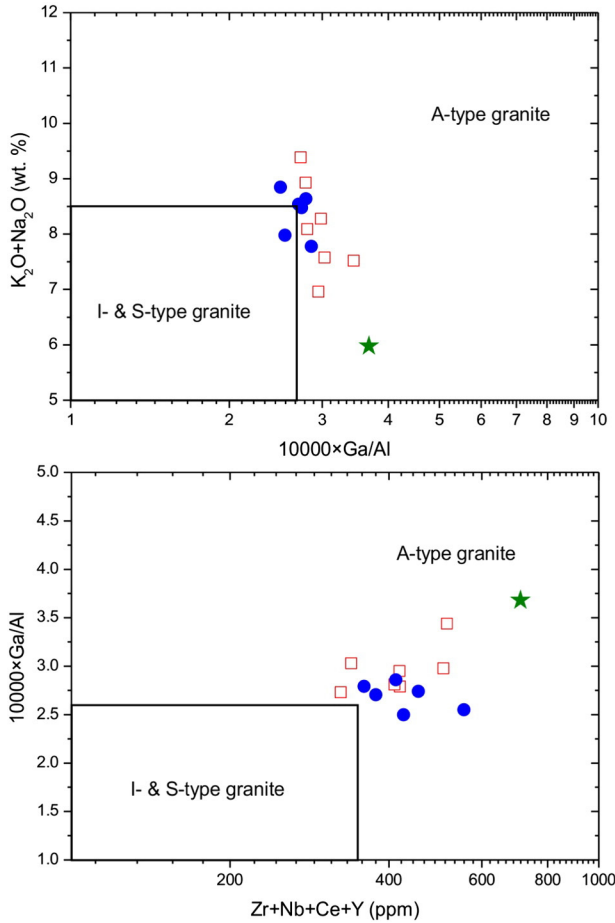


Fig. 9. Plots of $Na_2O + K_2O$ vs. $10,000 \times Ga/Al$ and $10,000 \times Ga/Al$ vs. $Zr + Nb + Ce + Y$ classification diagram of Whalen et al. (1987). Symbols are as in Fig. 5.

(Collins et al., 1982; Huang et al., 2011; Whalen et al., 1987; Zhao et al., 2013a), (3) low pressure incongruent melting of calc-alkaline rocks at upper crustal level (King et al., 1997; Patiño Douce, 1997), (4) melting of tholeiitic rocks newly derived from the mantle (Frost and Ronald Frost, 1997); and (5) hybridization between anatectic granitic and mantle-derived mafic magmas (Dahlquist et al., 2010; Kerr and Fryer, 1993; Mingram et al., 2000; Wickham et al., 1996; Yang et al., 2006; Zhao et al., 2012).

The Huitong and Epo granites have high A/CNK ratios and can be classed as peraluminous A-type granites. Alkaline and aluminous A-type granites are generally indicative of igneous source rocks, but

peraluminous A-type granites are uncommon (Dahlquist et al., 2014). The Huitong and Epo granites have strongly negative $\varepsilon_{Nd}(t)$ values (-10.4 to -7.7) and zircon $\varepsilon_{Hf}(t)$ values (peak value of -8.0), which implies that these granites were not directly derived from a mantle-derived mafic magma. High A/CNK ratios and low MgO contents also indicate that the granites came from partial melting of crustal rocks. The geochemical characteristics of the two granites are similar to those of Devonian peraluminous A-type granites in the Andean Achala batholith that are thought to be derived from a crustal source with a dominant metasedimentary component (Dahlquist et al., 2014).

The primary magma for the Huitong and Epo granites was anhydrous and had a high melting temperature, suggesting that the crustal sources had been dehydrated and/or melt depleted, and were either granulitic metavolcanic rocks or metasedimentary rocks (Collins et al., 1982). Creaser et al. (1991) suggested that the residual source remaining from generation of an I-type granite was unlikely to generate a partial melt with the appropriate major element characteristics of A-type granites. Hence, because the Nd isotopic compositions of the Huitong and Epo granites fall in the range of basement parametamorphic rocks in central Jiangxi Province, and are different from the basement orthometamorphic rocks (Fig. 11) (Hu and Zhang, 1998), we suggest that the parental magmas of the Huitong and Epo granites mainly originated from pre-Cambrian meta-sedimentary basement. Metasedimentary rocks may contain appropriate minerals and geochemical compositions required for A-type magmatism, as evidenced from the Ivrea zone of the south Alps, where granulite facies metapelites (stronalites) contain quartz, K-feldspar, plagioclase, and subordinate biotite (e.g. Bea and Montero, 1999). Partial melting of such rocks could thus produce peraluminous A-type magma.

Older and concordia ages (~ 445 Ma) were found in some zircon grains (Fig. 4). These zircon grains have high Th/U ratios (0.47–1.30), implying a magmatic origin. The ages are similar to the emplacement ages (434–451 Ma) of the nearby Fufang, Yingshang and Ninghua granites (Wang et al., 2011; Zhang et al., 2010). The $\varepsilon_{Hf}(t)$ values of the older zircons are fully consistent with the younger ones, suggesting an early magmatic origin from the same source. Thus, the source may have experienced an earlier melting and melt extraction event at about 445 Ma at the syn-collisional stage of the Wuyi–Yunkai orogeny. If, as seems likely, the source rocks were granulized during the thermal event (e.g. Yu et al., 2005), the Huitong and Epo granites may have formed from partial melting of the residual granulitic source remaining from this melt extraction at higher temperature at about 415 Ma.

7.3. Origin of MMEs

Mafic microgranular enclaves are widespread in granitic rocks and have been the focus of many studies (e.g. Didier and Barbarin,

Table 4
Sr-Nd isotopic compositions of the Huitong and Epo granites and the MMEs.

Sample	Age (Ma)	Rb (ppm)	Sr (ppm)	$^{87}\text{Rb}/^{86}\text{Sr}$	$^{87}\text{Sr}/^{86}\text{Sr}$	Error (2SE)	$(^{87}\text{Sr}/^{86}\text{Sr})_i$	Sm (ppm)	Nd (ppm)	$^{147}\text{Sm}/^{144}\text{Nd}$	$^{143}\text{Nd}/^{144}\text{Nd}$	Error (2SE)	$\varepsilon_{Nd}(t)$	T_{DM}^C
<i>Huitong granite</i>														
09HT-1	415	320.2	74.6	12.5	0.759517	0.000002	0.685763	8.61	48.69	0.107	0.511963	0.000004	-8.4	1.84
09HT-2	415	261.6	119.4	6.36	0.736877	0.000003	0.699312	10.96	57.82	0.115	0.511880	0.000007	-10.4	2.00
09HT-5	415	259.6	116.4	6.47	0.742521	0.000006	0.704269	8.61	48.10	0.108	0.511903	0.000006	-9.7	1.94
09HT-7	415	295.5	78.8	10.9	0.759732	0.000003	0.695297	5.61	29.20	0.116	0.511953	0.000005	-9.1	1.90
09HT-8	415	292.3	92.1	9.23	0.759891	0.000008	0.705362	8.00	42.79	0.113	0.511948	0.000013	-9.0	1.89
09HT-9a	415	226.9	195.2	3.37	0.731609	0.000009	0.711685	9.71	54.09	0.109	0.511921	0.000003	-9.3	1.91
09HT-10	415	245.2	192.6	3.69	0.734851	0.000006	0.713022	9.01	54.90	0.099	0.511919	0.000004	-8.9	1.88
<i>Epo granite</i>														
09EP-1	415	129.7	135.0	2.78	0.722693	0.000003	0.706240	7.71	40.01	0.116	0.511990	0.000010	-8.4	1.84
09EP-2a	415	215.4	220.8	2.83	0.732210	0.000004	0.715492	8.62	50.08	0.104	0.511963	0.000004	-8.3	1.83
09EP-4	415	170.0	144.6	3.41	0.734463	0.000003	0.714312	5.73	28.31	0.122	0.512041	0.000010	-7.7	1.78
<i>MME</i>														
09HT-9b	415	248.9	162.0	4.46	0.735601	0.000006	0.709268	12.06	63.30	0.115	0.512044	0.000004	-7.3	1.75

Table 5

Lu-Hf isotopic compositions of zircons from the Huitong and Epo granites and the MMEs.

Spot	Age (Ma)	$^{176}\text{Yb}/^{177}\text{Hf}$	$^{176}\text{Lu}/^{177}\text{Hf}$	$^{176}\text{Hf}/^{177}\text{Hf}$	2σ	$\epsilon_{\text{Hf}}(\text{t})$	C_{TDM} (Ma)
<i>Huitong granite HT-9a</i>							
HT-9a-01	418	0.030466	0.000942	0.282319	0.000022	-7.1	1853
HT-9a-02	415	0.061024	0.001843	0.282291	0.000025	-8.4	1933
HT-9a-03	418	0.059225	0.00182	0.282361	0.000025	-5.8	1775
HT-9a-04	416	0.036752	0.001067	0.28231	0.000019	-7.5	1878
HT-9a-05	418	0.050379	0.001485	0.282303	0.000021	-7.8	1899
HT-9a-06	414	0.055084	0.001676	0.282295	0.000019	-8.2	1922
HT-9a-07	413	0.046947	0.001383	0.282324	0.000021	-7.1	1854
HT-9a-08	415	0.032947	0.001035	0.282279	0.000022	-8.6	1947
HT-9a-09	415	0.047685	0.001477	0.282315	0.000026	-7.5	1874
HT-9a-10	415	0.064988	0.001821	0.282302	0.000024	-8.0	1909
HT-9a-11	412	0.040569	0.001257	0.282333	0.000023	-6.8	1831
HT-9a-12	412	0.054973	0.001682	0.282108	0.000027	-14.9	2340
HT-9a-13	418	0.049694	0.00144	0.282350	0.000029	-6.1	1792
HT-9a-14	415	0.035155	0.001028	0.282271	0.000022	-8.9	1965
HT-9a-15	415	0.042306	0.00127	0.282326	0.000021	-7.0	1845
HT-9a-16	415	0.0363	0.000992	0.282300	0.000018	-7.9	1900
HT-9a-17	415	0.057234	0.001673	0.282330	0.000024	-7.0	1844
HT-9a-18	416	0.058111	0.001799	0.282286	0.000025	-8.5	1944
HT-9a-19	415	0.039122	0.001138	0.282291	0.000024	-8.2	1921
HT-9a-20	415	0.046342	0.001398	0.282188	0.000024	-11.9	2155
HT-9a-21	415	0.044926	0.001317	0.282310	0.000024	-7.6	1883
HT-9a-22	415	0.039077	0.001216	0.282310	0.000031	-7.5	1880
HT-9a-23	415	0.059626	0.001735	0.282359	0.000024	-6.0	1781
HT-9a-24	415	0.033463	0.001143	0.282269	0.000026	-9.0	1971
<i>Epo granite EP-4</i>							
EP-4-01	444	0.026319	0.000853	0.282304	0.000034	-7.0	1870
EP-4-02	411	0.047155	0.001428	0.282297	0.000023	-8.1	1915
EP-4-03	413	0.03768	0.001203	0.282327	0.000025	-7.0	1843
EP-4-04	445	0.053114	0.001575	0.282279	0.000021	-8.1	1938
EP-4-05	415	0.021434	0.000662	0.282372	0.000019	-5.2	1733
EP-4-06	446	0.045013	0.001508	0.282211	0.000021	-10.5	2087
EP-4-07	444	0.021077	0.000666	0.282377	0.000022	-4.4	1704
EP-4-08	419	0.037801	0.00113	0.282410	0.000023	-3.9	1653
EP-4-09	416	0.032953	0.001035	0.282343	0.000021	-6.3	1802
EP-4-10	412	0.020885	0.000629	0.282364	0.00002	-5.5	1751
EP-4-11	414	0.018651	0.000567	0.282376	0.000021	-5.1	1723
EP-4-12	444	0.027322	0.000833	0.282272	0.000023	-8.2	1942
EP-4-13	443	0.019378	0.00061	0.282313	0.000020	-6.7	1847
EP-4-14	411	0.050961	0.001415	0.282313	0.000020	-7.6	1879
EP-4-15	408	0.029198	0.00088	0.282386	0.000019	-4.9	1710
EP-4-16	411	0.024776	0.000756	0.282386	0.000022	-4.8	1705
EP-4-17	415	0.018603	0.00059	0.282291	0.000025	-8.1	1912
EP-4-18	418	0.043035	0.00133	0.282292	0.000025	-8.1	1921
<i>MME HT-9b in Huitong granite</i>							
HT-9b-01	415	0.057196	0.001763	0.282316	0.000029	-7.5	1876
HT-9b-02	415	0.062632	0.001826	0.282282	0.000034	-8.7	1953
HT-9b-03	415	0.038835	0.001242	0.282349	0.000029	-6.2	1794
HT-9b-05	415	0.043641	0.001397	0.282274	0.000026	-8.9	1963
HT-9b-06	415	0.071625	0.002129	0.282322	0.000042	-7.4	1870
HT-9b-07	415	0.052593	0.001707	0.282246	0.000031	-10.0	2032
HT-9b-08	415	0.082965	0.002376	0.282434	0.00003	-3.5	1624
HT-9b-09	415	0.055835	0.001612	0.282265	0.000059	-9.2	1986
HT-9b-10	415	0.048348	0.00142	0.282199	0.000051	-11.5	2131
HT-9b-11	415	0.050016	0.001564	0.282373	0.000039	-5.4	1745
HT-9b-12	415	0.082154	0.001872	0.282243	0.000056	-10.1	2040

1991), but there are considerable discrepancies between the models proposed to explain their origin, including whether they are restites of source rocks (Chappell et al., 1987; White et al., 1999), wall-rock xenoliths (Maas et al., 1997), early crystal-melt segregations (Dahlquist, 2002; Donaire et al., 2005) or products of mixing and mingling of different source-derived magmas (Barbarin, 2005; Didier and Barbarin, 1991; Perugini et al., 2003; Vernon, 1984; Zhao et al., 2012).

The enclaves in the Huitong granite have igneous microtextures (Fig. 3), and the presence of K-feldspar megacrysts in the enclaves is interpreted as proof that they were in a liquid state when incorporated into a more silicic magma (e.g. Vernon et al., 1988; Perugini et al.,

2003). Acicular apatite in the enclaves implies a rapid cooling crystallization process for the mafic magma (e.g. Sparks and Marshall, 1986; Vernon et al., 1988). Zircons from the enclaves are smaller in size than those from the host granite (Fig. 4). They have the same crystallization ages as those from the host granite. All these characteristics are similar to those of MMEs originating from magma mingling (e.g. Vernon et al., 1988; Perugini et al., 2003; Zhao et al., 2012). These observations thus argue against the interpretation that these enclaves are restites or xenoliths, and suggest that magma mingling of different source-derived magmas took place in the genesis of the granite; i.e. the MMEs and the host granite formed from different source-derived magmas.

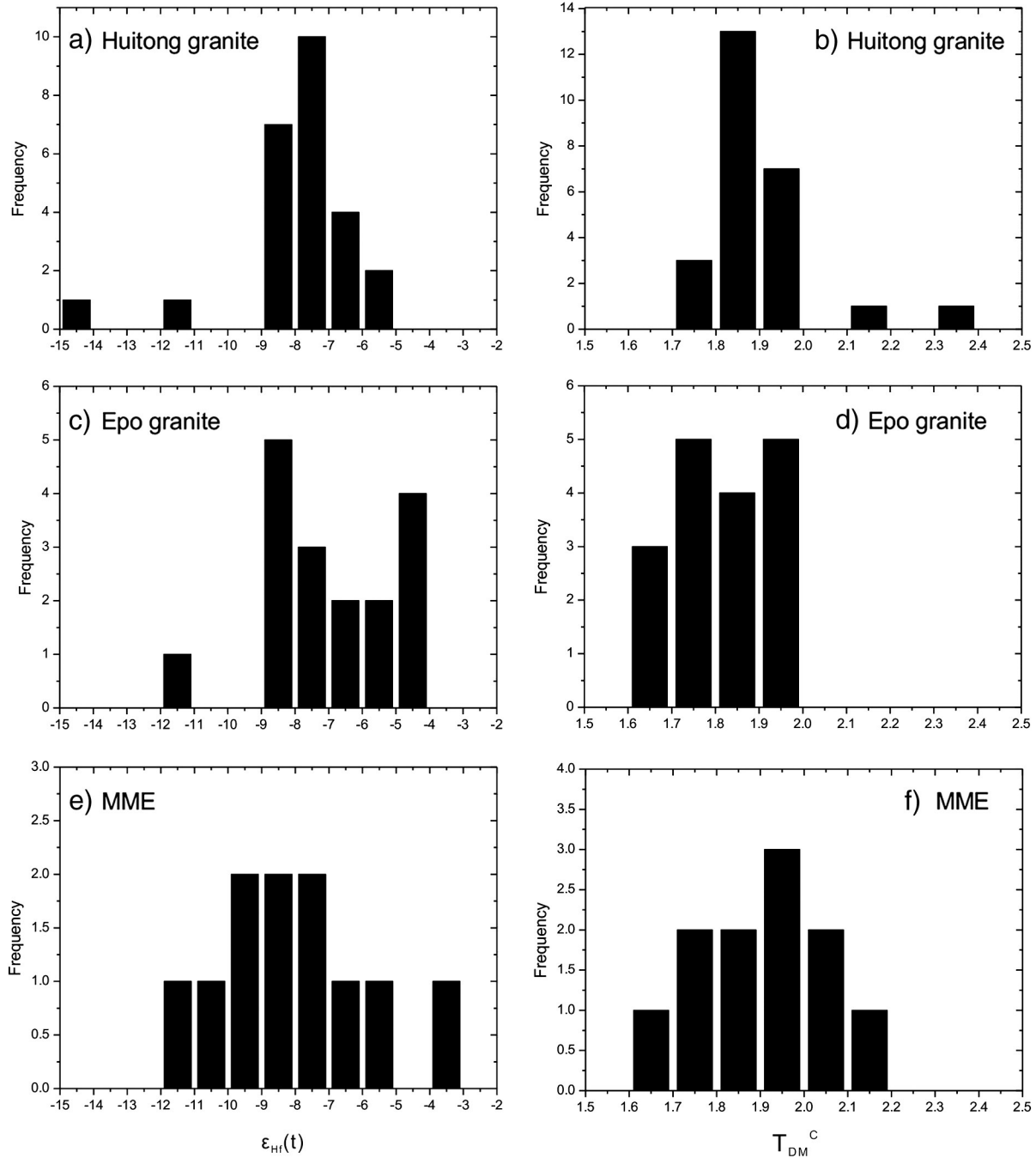


Fig. 10. Histograms of zircon $\epsilon_{\text{Hf}}(t)$ values and two-stage model ages (T_{DM}^{C}) of the Huitong and Epo granites and the MMEs.

The elemental and isotopic compositions of the MMEs are largely consistent with their host granite, which likely reflects some contamination of the MMEs by host magma by chemical diffusion. Thus, it is difficult to directly constrain the sources of MME magma end-member. The primary magma for MMEs in granites has generally been suggested to be derived from mantle sources (e.g. Barbarin, 2005; Didier and Barbarin, 1991; Zhao et al., 2012). The MMEs in the Huitong granite show relatively higher MgO contents, and higher Sc, V, Cr, Ni and Mo contents than the host granite (Table 3), which may indicate a mantle source. However, negative $\epsilon_{\text{Nd}}(t)$ values and zircon $\epsilon_{\text{Hf}}(t)$ values imply that the MMEs did not form directly from partial melting of the asthenospheric mantle. The Huitong and Epo A-type granites formed from the granulitic crustal basement. Thus, we suggested that the primary magma for the MMEs may have

formed from partial melting of underlying enriched lithospheric mantle.

7.4. Implication for tectonic-magmatic evolution of the Wuyi-Yunkai orogeny

According to previous studies, the early Paleozoic Wuyi-Yunkai orogeny in South China was likely an intraplate orogenic event (Fig. 1, e.g. Shu et al., 2008; Faure et al., 2009; Li et al., 2010; Charvet et al., 2010; He et al., 2010b; Charvet, 2013). The orogeny is characterized by widespread high-grade metamorphic rocks and granites, but little is known about the temporal-spatial evolution of the granitic magmatism responding to the orogenic processes. The early-middle Paleozoic granites are widespread throughout the Wuyi-Yunkai

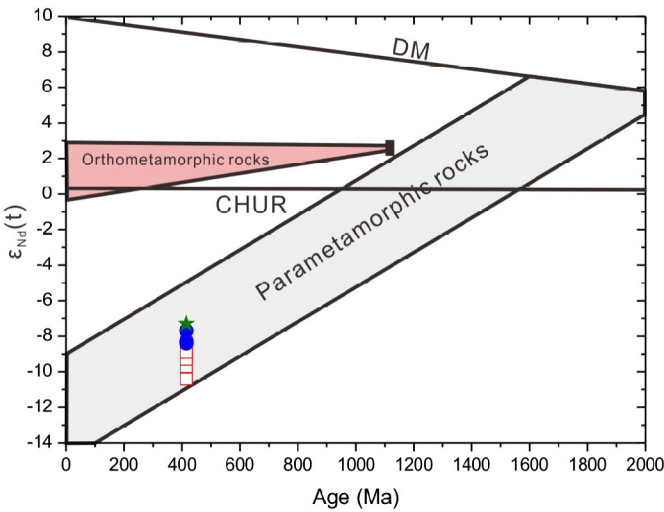


Fig. 11. Evolution of $\varepsilon_{\text{Nd}}(t)$ values vs. time of the Huitong and Epo granites, MMEs and the metamorphic basement in Central Jiangxi Province. Data of parametamorphic rocks in the basement are from Hu and Zhang (1998). Data of orthometamorphic rocks in the basement are from Hu et al. (1999). Symbols are as in Fig. 5.

orogeny, and have a wide age range of ca. 462–381 Ma (e.g. Li et al., 2010; Wang et al., 2012; Xia et al., 2014; Zhao et al., 2013a). Most of these are peraluminous S-type granites, except for a few occurrences that are considered as I-type granites. According to their petrography,

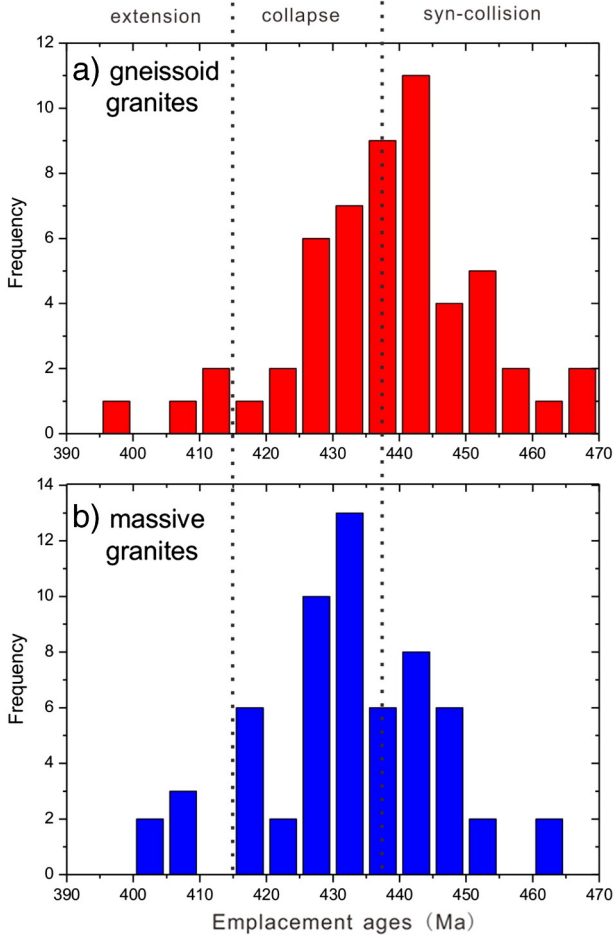


Fig. 12. Frequency of emplacement ages for the early-middle Paleozoic gneissoid (a) and massive (b) granites in eastern SCB. Data are from Table 2 in Wang et al. (2013a, 2013b).

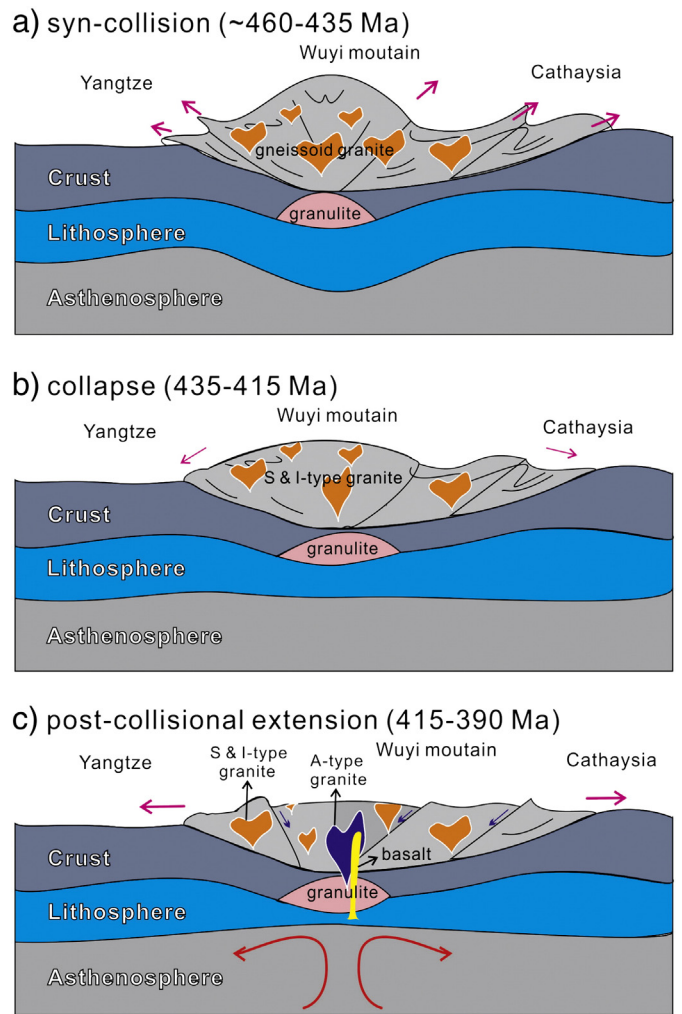


Fig. 13. Tectonic-magmatic models for the generation of the early-middle Paleozoic granites and the evolution of the Wuyi-Yunkai orogeny in eastern SCB. See the text for the details.

these granites can be classified into two types: gneissoid and massive. Age data imply that the gneissoid granites formed at 410–462 Ma, with a peak age of 440 Ma (Fig. 12). Massive granites statistically give zircon U-Pb ages ranging from 382 Ma to 458 Ma, with a peak age of 430 Ma, which is 10 Ma younger than that of the gneissoid granites (Fig. 12). We suggested that most of the gneissoid granites formed in the syn-collisional environment with crustal thickening leading to high heat production in the source, and that most of the massive granites formed during the orogenic collapse stage.

This study is the first to identify Devonian A-type granites in the Wuyi-Yunkai Orogeny. As noted above, A-type granites can form in a variety of extensional tectonic environments (e.g., continental arc, back arc extension, post-collisional extension and within-plate settings) regardless of the origin of the magma source (e.g. Bonin, 2007; Eby, 1992; Loiselle and Wones, 1979; Turner et al., 1992; Whalen et al., 1987). The Huitong-Epo granites are peraluminous A-type granites formed from crustal reworking, thus an origin related to a hot spot, plume or continental rift zone located in anorogenic settings is unlikely, and a post-collisional extension environment is a more likely scenario.

Together with results from previous studies, the results presented here suggest that the genesis of the Paleozoic granites in South China can be separated into three stages (Fig. 13). In the first stage (~460 Ma to 435 Ma), most gneissoid granites formed in a syn-collisional compression setting from dehydrated melting of crustal rocks during crust thickening. At the same time, the deep crustal rocks

experienced melt-extraction and they were granitized. In the second stage (435 Ma to 415 Ma), most massive granites formed as a result of the collapse of the orogeny. These granites are peraluminous S-type and I-type, and originated from melting Proterozoic pelite and igneous rocks. In the third stage from 415 Ma, the tectonic regime changed to a strongly post-collisional extension environment in which rapid crustal thinning and underplating of hot mantle magma induced the melting of the orogenic root and crust–mantle interaction. A-type granites and mafic magmatism formed along the extensional zones and other I/S granites formed away from the zones. Thus, at least from 415 Ma, the Wuyi–Yunkai orogeny in South China changed from a syn-collisional setting to a post-collisional extensional setting.

8. Conclusions

- (1) LA-ICP-MS zircon U–Pb geochronology indicated that the Huitong granite was emplaced at 415 ± 3 Ma, and the Epo granite was emplaced at 414 ± 3 Ma.
- (2) Petrologic, geochemical and isotopic data demonstrate that the Huitong and Epo granites belong to peraluminous A-type classification. They were derived from partial melting of pre-Cambrian sedimentary rocks that had been granitized during an earlier thermal event.
- (3) Mafic microgranular enclaves in the granites originated from magma mingling and the primary magma may have been derived from the underlying enriched lithospheric mantle.
- (4) The presence of Devonian A-type granites and MMEs imply the existence of a post-collisional extension setting at 415 Ma. Thus, the Wuyi–Yunkai orogeny in South China changed from syn-collisional crustal thickening to post-collisional extension after 415 Ma.

Supplementary data to this article can be found online at <http://dx.doi.org/10.1016/j.lithos.2014.07.007>.

Acknowledgments

This work is supported by projects from the Major State Basic Research Program of China (2012CB406700), National Natural Science Foundation of China (No. 41273038), China Nuclear Geological Bureau (YK11) and Ministry of Education of the People's Republic of China (No. 306007). Kui-Dong Zhao is also grateful for the financial support from the China Scholarship Council (201208320113). Thorough reviews by Dr. Juan A. Dahlquist, Dr. Zhen-Yu He and the Editor-in-Chief, Professor Nelson Eby resulted in a major improvement of the original manuscript. Professor Martin Palmer at the University of Southampton helps to correct the language errors. We are grateful to them.

References

- Abdel-Rahman, A.F.M., 1994. Nature of biotites from alkaline, calc-alkaline, and peraluminous magmas. *Journal of Petrology* 35 (2), 525–541.
- Andersen, T., 2002. Correction of common Pb in U–Pb analyses that do not report ^{204}Pb . *Chemical Geology* 192, 59–79.
- Barbarin, B., 2005. Mafic magmatic enclaves and mafic rocks associated with some granitoids of the central Sierra Nevada batholith, California: nature, origin, and relations with the hosts. *Lithos* 80 (1–4), 155–177.
- Bea, F., Montero, P., 1999. Behavior of accessory phases and redistribution of Zr, REE, Y, Th and U during metamorphism and partial melting of metapelites in the lower crust: an example from the Kinzigite Formation of Ivrea-Verbano, NW Italy. *Geochimica et Cosmochimica Acta* 63, 1133–1153.
- Blichert-Toft, J., Albarède, F., 1997. The Lu-Hf isotope geochemistry of chondrites and the evolution of the mantle–crust system. *Earth and Planetary Science Letters* 148 (1–2), 243–258.
- Bonin, B., 2007. A-type granites and related rocks: evolution of a concept, problems and prospects. *Lithos* 97 (1–2), 1–29.
- Boynton, W.L., 1984. Geochemistry of the rare earth elements: meteorite studies. In: Henderson, P. (Ed.), *Rare Earth Element Geochemistry*. Elsevier, Amsterdam, pp. 63–114.
- Chappell, B.W., 1999. Aluminium saturation in I- and S-type granites and the characterization of fractionated haplogranites. *Lithos* 46 (3), 535–551.
- Chappell, B.W., White, A.J.R., 1974. Two contrasting granite types. *Pacific Geology* 8, 173–174.
- Chappell, B.W., White, A.J.R., Wyborn, D., 1987. The importance of residual source material (restite) in granite petrogenesis. *Journal of Petrology* 28 (6), 1111–1138.
- Charvet, J., 2013. The Neoproterozoic–Early Paleozoic tectonic evolution of the South China Block: an overview. *Journal of Asian Earth Sciences* 74, 198–209.
- Charvet, J., Shu, L., Faure, M., Choulet, F., Wang, B., Lu, H., Breton, N.L., 2010. Structural development of the Lower Paleozoic belt of South China: genesis of an intracontinental orogen. *Journal of Asian Earth Sciences* 39 (4), 309–330.
- Chen, B., Zhuang, Y.X., 1994. The petrology and petrogenesis of Yunlu chemockite and its granulite inclusion, west Guangdong, South China. *Acta Petrologica Sinica* 10 (2), 139–150 (in Chinese with English abstract).
- Chu, N.C., Taylor, R.N., Chavagnac, V., Nesbit, R.W., Boella, R.M., Milton, J.A., German, C.R., Bayon, G., Burton, K., 2002. Hf isotope ratio analysis using multi-collector inductively coupled plasma mass spectrometry: an evaluation of isobaric interference corrections. *Journal of Analytical Atomic Spectrometry* 17, 1567–1574.
- Clemens, J.D., 2003. S-type granitic magmas—petrogenetic issues, models and evidence. *Earth-Science Reviews* 61 (1–2), 1–18.
- Collins, W.J., Beams, S.D., White, A.J.R., Chappell, B.W., 1982. Nature and origin of A-type granites with particular reference to southeastern Australia. *Contribution to Mineralogy and Petrology* 80, 189–200.
- Creaser, R.A., Price, R.C., Wormald, R.J., 1991. A-type granites revisited: assessment of a residual-source model. *Geology* 19 (2), 163–166.
- Dahlquist, J.A., 2002. Mafic microgranular enclaves: early segregation from metaluminous magma (Sierra de Chepes), Pampean Ranges, NW Argentina. *Journal of South American Earth Sciences* 15 (6), 643–655.
- Dahlquist, J.A., Alasino, P.H., Eby, G.N., Galindo, C., Casquet, C., 2010. Fault controlled Carboniferous A-type magmatism in the proto-Andean foreland (Sierras Pampeanas, Argentina): geochemical constraints and petrogenesis. *Lithos* 115 (1), 65–81.
- Dahlquist, J.A., Alasino, P.H., Bello, C., 2014. Devonian F-rich peraluminous A-type magmatism in the proto-Andean foreland (Sierras Pampeanas, Argentina): geochemical constraints and petrogenesis from the western-central region of the Achala batholith. *Mineralogy and Petrology* 108 (3), 391–417.
- Didier, J., Barbarin, B., 1991. Encalves and granite petrology. *Developments in Petrology*, 13. Elsevier, Amsterdam, pp. 1–625.
- Donaire, T., Pascual, E., Pin, C., Duthou, J.-L., 2005. Microgranular enclaves as evidence of rapid cooling in granitoid rocks: the case of the Los Pedrosches granodiorite, Iberian Massif, Spain. *Contributions to Mineralogy and Petrology* 149 (3), 247–265.
- Eby, G.N., 1992. Chemical subdivision of the A-type granitoids: petrogenetic and tectonic implications. *Geology* 20, 641–644.
- Faure, M., Shu, L., Wang, B., Charvet, J., Choulet, F., Monie, P., 2009. Intracontinental subduction: a possible mechanism for the Early Palaeozoic Orogen of SE China. *Terra Nova* 21 (5), 360–368.
- Förster, H.J., Tischendorf, G., Trumbull, R.B., 1997. An evaluation of the Rb vs (Y + Nb) discrimination diagram to infer tectonic setting of silicic igneous rocks. *Lithos* 40, 261–293.
- Frost, C.D., Ronald Frost, B., 1997. Reduced rapakivi-type granites: the tholeiite connection. *Geology* 25 (7), 647.
- Gao, J.F., Lu, J.J., Lai, M.Y., Lin, Y.P., Pu, W., 2003. Analysis of trace elements in rock samples using HR-ICPMS. *Journal of Nanjing University (Nature Sciences)* 39, 844–850 (in Chinese with English abstract).
- Gilder, S.A., Keller, G.R., Luo, M., Goodell, P.C., 1991. Timing and spatial distribution of rifting in China. *Tectonophysics* 197, 225–243.
- Griffin, W.L., Wang, X., Jackson, S.E., Pearson, N.J., O'Reilly, S.Y., Xu, X., Zhou, X., 2002. Zircon chemistry and magma mixing, SE China: in-situ analysis of Hf isotopes, Tonglu and Pingtan igneous complexes. *Lithos* 61 (3–4), 237–269.
- He, Z.Y., Xu, X.S., Niu, Y., 2010a. Petrogenesis and tectonic significance of a Mesozoic granite–syenite–gabbro association from inland South China. *Lithos* 119 (3–4), 621–641.
- He, Z.Y., Xu, X.S., Zou, H.B., Wang, X.D., Yu, Y., 2010b. Geochronology, petrogenesis and metallogeny of Piaotang granitoids in the tungsten deposit region of South China. *Geochemical Journal* 44 (4), 299–313.
- Hoskin, P.W.O., Schaltegger, U., 2003. The compositions of zircon and igneous and metamorphic petrogenesis. *Reviews in Mineralogy and Geochemistry* 53, 27–55.
- Hsü, K.J., Sun, S., Li, J.L., Chen, H.H., Pen, H.P., Sengor, A.M.C., 1988. Mesozoic overthrust tectonics in South China. *Geology* 16, 421–428.
- Hu, G.R., Zhang, B.T., 1998. Neodymium isotope composition and source materials of the metabasement in Central Jiangxi Province. *Acta Petrologica et Mineralogica* 17 (1), 35–40 (in Chinese with English abstract).
- Hu, G.R., Zhang, B.T., 1999. Preliminary study on the Nd-isotopic model ages and the formation age of the metamorphic basement in Central Jiangxi. *Uranium Geology* 15 (3), 137–141 (in Chinese with English abstract).
- Hu, G.R., Zhang, B.T., Yu, R.L., 1999. A study on Sm-Nd and Rb-Sr isochron ages of the Central Jiangxi metamorphic belt. *Geological Review* 45 (2), 129–134 (in Chinese with English abstract).
- Huang, T.K., 1978. An outline of the tectonic characteristics of China. *Eclogae Geologicae Helvetiae* 71, 611–635.
- Huang, H.Q., Li, X.H., Li, W.X., Li, Z.X., 2011. Formation of high ^{18}O fayalite-bearing A-type granite by high-temperature melting of granulitic metasedimentary rocks, southern China. *Geology* 39 (10), 903–906.
- Jackson, S.E., Pearson, N.J., Griffin, W.L., Belousova, E.A., 2004. The application of laser ablation inductively coupled plasma mass spectrometry to in situ U-Pb zircon geochronology. *Chemical Geology* 211, 47–69.
- Jacobsen, S.B., Wasserburg, G.J., 1980. Sm-Nd isotopic evolution of chondrites. *Earth and Planetary Science Letter* 50, 139–155.

- Jahn, B.M., Condie, K.C., 1995. Evolution of the Kaapvaal Craton as viewed from geochemical and Sm–Nd isotopic analyses of intracratonic pelites. *Geochimica et Cosmochimica Acta* 59 (11), 2239–2258.
- Jiang, Y.H., Jiang, S.Y., Dai, B.Z., Liao, S.Y., Zhao, K.D., Ling, H.F., 2009. Middle to late Jurassic felsic and mafic magmatism in southern Hunan province, southeast China: implications for a continental arc to rifting. *Lithos* 107 (3–4), 185–204.
- Jung, S., Pfänder, J.A., 2007. Source composition and melting temperatures of orogenic granitoids: constraints from CaO/Na₂O, Al₂O₃/TiO₂ and accessory mineral saturation thermometry. *European Journal of Mineralogy* 19, 859–870.
- Kerr, A., Fryer, B.J., 1993. Nd isotope evidence for crust–mantle interaction in the generation of A-type granitoid suites in Labrador, Canada. *Chemical Geology* 104 (1–4), 39–60.
- King, P.L., White, A.J.R., Chappell, B.W., Allen, C.M., 1997. Characterization and origin of aluminous A-type granites from the Lachlan Fold Belt, Southeastern Australia. *Journal of Petrology* 38 (3), 371–391.
- King, P.L., Chappell, B.W., Allen, C.M., White, A.J.R., 2001. Are A-type granites the high-temperature felsic granites? Evidence from fractionated granites of the Wangrah Suite. *Australian Journal of Earth Sciences* 48, 501–514.
- Li, Z.X., Li, X.H., 2007. Formation of the 1300-km-wide intracontinental orogen and postorogenic magmatic province in Mesozoic South China: a flat-slab subduction model. *Geology* 35 (2), 179–182.
- Li, X.H., Li, W.X., Li, Z.X., 2007. On the genetic classification and tectonic implications of the early Yanshanian granitoids in the Nanling Range, South China. *Chinese Science Bulletin* 52 (14), 1873–1885.
- Li, X.H., Li, W.X., Li, Z.X., Lo, C.H., Wang, J., Ye, M.F., Yang, Y.H., 2009. Amalgamation between the Yangtze and Cathaysia Blocks in South China: Constraints from SHRIMP U–Pb zircon ages, geochemistry and Nd–Hf isotopes of the Shuangxiwu volcanic rocks. *Precambrian Research* 174 (1–2), 117–128.
- Li, Z.X., Li, X.H., Wartho, J.A., Clark, C., Li, W.X., Zhang, C.L., Bao, C., 2010. Magmatic and metamorphic events during the early Paleozoic Wuyi–Yunkai orogeny, southeastern South China: new age constraints and pressure–temperature conditions. *Geological Society of America Bulletin* 122 (5–6), 772–793.
- Litvinovsky, B.A., Jahn, B.M., Zavilevich, A.N., Saunders, A., Poulain, S., Kuzmin, D.V., Reichow, M.K., Titov, A.V., 2002. Petrogenesis of syenite–granite suites from the Bryansk Complex (Transbaikalia, Russia): implications for the origin of A-type granitoid magmas. *Chemical Geology* 189 (1–2), 105–133.
- Loiselle, M.C., Wones, D.R., 1979. Characteristics and origin of anorogenic granites. Abstracts of papers to be presented at the Annual Meetings of the Geological Society of America and Associated Societies, San Diego, California, November 5–8, 11, p. 468.
- Lugmair, G.W., Marti, K., 1978. Lunar initial $^{143}\text{Nd}/^{144}\text{Nd}$: differential evolution of the lunar crust and mantle. *Earth and Planetary Science Letter* 39, 349–357.
- Maas, R., Nicholls, I.A., Legg, C., 1997. Igneous and metamorphic enclaves in the S-type Dedick Granodiorite, Lachlan Fold Belt, SE Australia: petrographic, geochemical and Nd–Sr isotopic evidence for crustal melting and magma mixing. *Journal of Petrology* 38 (7), 815–841.
- Miller, C.F., McDowell, S.M., Mapes, R.W., 2003. Hot and cold granites? Implications of zircon saturation temperatures and preservation of inheritance. *Geology* 31 (6), 529–532.
- Mingram, B., Trumbull, R.B., Littman, S., Gerstenberger, H., 2000. A petrogenetic study of anorogenic felsic magmatism in the Cretaceous Paresis ring complex, Namibia: evidence for mixing of crust and mantle-derived components. *Lithos* 54 (1–2), 1–22.
- Morel, M.L.A., Nebel, O., Nebel-Jacobsen, Y.J., Miller, J.S., Vroon, P.Z., 2008. Hafnium isotope characterization of the GJ-1 zircon reference material by solution and laser-ablation MC-ICPMS. *Chemical Geology* 255 (1–2), 231–235.
- Mushkin, A., Navon, O., Halicz, L., Hartmann, G., Stein, M., 2003. The petrogenesis of A-type magmas from the Amram Massif, Southern Israel. *Journal of Petrology* 44 (5), 815–832.
- Patrón Douce, A.E., 1997. Generation of metaluminous A-type granites by low-pressure melting of calc-alkaline granitoids. *Geology* 25, 743–746.
- Peng, S.B., Jin, Z.M., Fu, J.M., Liu, Y.H., He, L.Q., Cai, M.H., 2006a. Geochemical characteristics of basic intrusive rocks in the Yunkai uplift, Guangdong–Guangxi, China, and their tectonic significance. *Geological Bulletin of China* 25 (4), 434–441 (in Chinese with English abstract).
- Peng, S.B., Jin, Z.M., Liu, Y.H., Fu, J.M., He, L.Q., Cai, M.H., Wang, Y.B., 2006b. Petrochemistry, chronology and tectonic settings of strong peraluminous anatexitic granitoids in Yunkai Orogenic Belt, western Guangdong Province, China. *Earth Science–Journal of China University of Geosciences* 31 (1), 110–120 (in Chinese with English abstract).
- Perugini, D., Poli, G., Christofides, G., Eleftheriadis, G., 2003. Magma mixing in the Sithonia Plutonic Complex, Greece: evidence from mafic microgranular enclaves. *Mineralogy and Petrology* 78 (3), 173–200.
- Pu, W., Zhao, K.D., Ling, H.F., Jiang, S.Y., 2004. High precision Nd isotope measurement by Triton Ti mass spectrometry. *Acta Geoscientifica Sinica* 25, 271–274 (in Chinese with English abstract).
- Pu, W., Gao, J.F., Zhao, K.D., Ling, H.F., Jiang, S.Y., 2005. Separation method of Rb–Sr, Sm–Nd using DCTA and HIBA. *Journal of Nanjing University (Nature Sciences)* 41, 445–450 (in Chinese with English abstract).
- Ren, J., 1964. A preliminary study on pre-Devonian geotectonic problems of southeastern China. *Acta Geologica Sinica* 44 (4), 418–431 (in Chinese).
- Ren, J., 1991. On the geotectonics of southern China. *Acta Geologica Sinica – English Edition* 4 (2), 111–130.
- Scherer, E., Munker, C., Mezger, K., 2001. Calibration of the lutetium–hafnium clock. *Science* 293 (5530), 683–687.
- Shen, W.Z., Zhang, F.R., Shu, L.S., Wang, L.J., Xiang, L., 2008. Formation age, geochemical characteristics of the Ninggang granite body in Jiangxi Province and its tectonic significance. *Acta Petrologica Sinica* 24 (10), 2244–2254 (in Chinese with English abstract).
- Shu, L.S., Yu, J.H., Jia, D., Wang, B., Shen, W., Zhang, Y.Q., 2008. Early Paleozoic orogenic belt in the eastern segment of South China. *Geological Bulletin of China* 27, 1581–1593 (in Chinese with English abstract).
- Sparks, R.S.J., Marshall, L., 1986. Thermal and mechanical constraints on mixing between mafic and silicic magmas. *Journal of Volcanology and Geothermal Research* 29, 99–124.
- Sun, S.S., McDonough, W.F., 1989. Chemical and isotopic systematics of oceanic basalt: Implications for mantle composition and processes. *Geological Society, London, Special Publication* 42, 528–548.
- Tanaka, T., Togashi, S., Kamioka, H., Amakawa, H., Kagami, H., Hamamoto, T., Yuhara, M., Orihashi, Y., Yoneda, S., Shimizu, H., Kunimaru, T., Takahashi, K., Yanagi, T., Nakano, T., Fujimaki, H., Shinjo, R., Asahara, Y., Tanimizu, M., Dragusanu, C., 2000. JNdI-1: a neodymium isotopic reference in consistency with LaJolla neodymium. *Chemical Geology* 168 (3–4), 279–281.
- Ting, W.K., 1929. The orogenic movement in China. *Geological Society of China* 8 (1), 151–170 (in Chinese).
- Turner, S.P., Foden, J.D., Morrison, R.S., 1992. Derivation of some A-type magmas by fractionation of basaltic magma: an example from the Padthaway Ridge, South Australia. *Lithos* 28 (2), 151–179.
- Van Achterbergh, E., Ryan, C.G., Jackson, S.E., Griffin, W.L., 2001. Data reduction software for La-ICP-MS: appendix. In: Sylvester, P.J. (Ed.), *Laser Ablation–ICP–Mass-Spectrometry in the Earth Sciences: Principles and Applications*. Mineralogist Association Canada Short Course Series, Ottawa, pp. 239–243.
- Vernon, R.H., 1984. Microgranitoid enclaves in granites: globules of hybrid magma quenched in a plutonic environment. *Nature* 309, 438–439.
- Vernon, R.H., Etheridge, M.A., Wall, V.J., 1988. Shape and microstructure of microgranitoid enclaves: Indicators of magma mingling and flow. *Lithos* 22 (1), 1–11.
- Wan, Y., Liu, D., Xu, M., Zhuang, J., Song, B., Shi, Y., Du, L., 2007. SHRIMP U–Pb zircon geochronology and geochemistry of metavolcanic and metasedimentary rocks in Northwestern Fujian, Cathaysia block, China: tectonic implications and the need to redefine lithostratigraphic units. *Gondwana Research* 12 (1–2), 166–183.
- Wan, Y., Liu, D., Wilde, S.A., Cao, J., Chen, B., Dong, C., Song, B., Du, L., 2010. Evolution of the Yunkai Terrane, South China: evidence from SHRIMP zircon U–Pb dating, geochemistry and Nd isotope. *Journal of Asian Earth Sciences* 37 (2), 140–153.
- Wang, J., Li, Z.X., 2003. History of Neoproterozoic rift basins in South China: implications for Rodinia break-up. *Precambrian Research* 122 (1–4), 141–158.
- Wang, D.Z., Zhou, J.C., 2005. New progress in studying the Large Igneous Provinces. *Geological Journal of China Universities* 11 (1), 1–8 (in Chinese with English abstract).
- Wang, Y.J., Fan, W.M., Zhao, G.C., Ji, S.C., Peng, T.P., 2007. Zircon U–Pb geochronology of gneissic rocks in the Yunkai massif and its implications on the Caledonian event in the South China Block. *Gondwana Research* 12 (4), 404–416.
- Wang, Y.J., Zhang, A.M., Fan, W.M., Zhao, G.C., Zhang, G.W., Zhang, Y.Z., Zhang, F.F., Li, S.Z., 2011. Kwangssian crustal anatexis within the eastern South China Block: geochemical, zircon U–Pb geochronological and Hf isotopic fingerprints from the gneissoid granites of Wugong and Wuyi–Yunkai Domains. *Lithos* 127 (1–2), 239–260.
- Wang, Y.J., Wu, C.M., Zhang, A.M., Fan, W.M., Zhang, Y.H., Zhang, Y.Z., Peng, T.P., Yin, C.Q., 2012. Kwangssian and Indosian reworking of the eastern South China Block: constraints on zircon U–Pb geochronology and metamorphism of amphibolites and granulites. *Lithos* 150, 227–242.
- Wang, Y.J., Fan, W.M., Zhang, G.W., Zhang, Y.H., 2013a. Phanerozoic tectonics of the South China Block: key observations and controversies. *Gondwana Research* 23 (4), 1273–1305.
- Wang, Y.J., Zhang, A.M., Fan, W.M., Zhang, Y.H., Zhang, Y.Z., 2013b. Origin of paleosubduction-modified mantle for Silurian gabbro in the Cathaysia Block: geochronological and geochemical evidence. *Lithos* 160–161, 37–54.
- Watson, E.B., Harrison, T.M., 1983. Zircon saturation revisited: temperature and composition effects in a variety of crustal magma types. *Earth and Planetary Science Letters* 64, 295–304.
- Whalen, J.B., Currie, K.L., Chappell, B.W., 1987. A-type granites: geochemical characteristics, discrimination and petrogenesis. *Contributions to Mineralogy and Petrology* 95 (4), 407–419.
- White, A.J.R., Chappell, B.W., Wyborn, D., 1999. Application of the restite model to the Dedick granodiorite and its enclaves – a reinterpretation of the observations and data of Maas et al. (1997). *Journal of Petrology* 40 (3), 413–421.
- Wickham, S.M., Alberts, A.D., Zavilevich, A.N., Litvinovsky, B.A., Bindeman, I.N., Schauble, E.A., 1996. A stable isotope study of anorogenic magmatism in East Central Asia. *Journal of Petrology* 37 (5), 1063–1095.
- Wright, J.B., 1969. A simple alkalinity ratio and its application to questions of nonorogenic granite genesis. *Geological Magazine* 106, 370–384.
- Wu, Y.B., Zheng, Y.F., 2004. Genesis of zircon and its constraints on interpretation of U–Pb age. *Chinese Science Bulletin* 49 (15), 1554–1569.
- Wu, F.Y., Yang, Y.H., Xie, L.W., Yang, J.H., Xu, P., 2006. Hf isotopic compositions of the standard zircons and baddeleyites used in U–Pb geochronology. *Chemical Geology* 234 (1–2), 105–126.
- Wu, F.Y., Li, X.H., Yang, J.H., Zheng, Y.F., 2007. Discussions on the petrogenesis of granites. *Acta Petrologica Sinica* 23 (6), 1217–1238 (in Chinese with English abstract).
- Xia, Y., Xu, X., Zou, H., Liu, L., 2014. Early Paleozoic crust–mantle interaction and lithosphere delamination in South China Block: evidence from geochronology, geochemistry, and Sr–Nd–Hf isotopes of granites. *Lithos* 184–187, 416–435.
- Xu, X.B., Zhang, Y.Q., Shu, L.S., Jia, D., Wang, R.R., Xu, H.Z., 2009. Zircon LA-ICPMS U–Pb dating of the Weipu granitic pluton in Southwest Fujian and the Changpu Metamorphic in South Jiangxi: constraints to the timing of Caledonian Movement in Wuyi Mountains. *Geological Reviews* 55 (2), 277–285 (in Chinese with English abstract).
- Xu, X.B., Zhang, Y.Q., Shu, L.S., Jia, D., 2011. La-ICP-MS U–Pb and $^{40}\text{Ar}/^{39}\text{Ar}$ geochronology of the sheared metamorphic rocks in the Wuyishan: constraints on the timing of Early

- Paleozoic and Early Mesozoic tectono-thermal events in SE China. *Tectonophysics* 501 (1–4), 71–86.
- Yang, J.H., Wu, F.Y., Chung, S.L., Wilde, S.A., Chu, M.F., 2006. A hybrid origin for the Qianshan A-type granite, northeast China: geochemical and Sr–Nd–Hf isotopic evidence. *Lithos* 89 (1–2), 89–106.
- Yang, S.Y., Jiang, S.Y., Zhao, K.D., Jiang, Y.H., Ling, H.F., Luo, L., 2012. Geochronology, geochemistry and tectonic significance of two Early Cretaceous A-type granites in the Gan-Hang Belt, Southeast China. *Lithos* 150, 155–170.
- Yu, J.H., Zhou, X.M., Zhao, L., Chen, X.M., 2003. Discovery and implications of granulite facies metamorphic rocks in the eastern Nanling, China. *Acta Petrologica Sinica* 19 (3), 461–467 (in Chinese with English abstract).
- Yu, J.H., Zhou, X.M., O'Reilly, S.Y., 2005. Formation history and protolith characteristics of granulite facies metamorphic rock in Central Cathaysia deduced from U–Pb and Lu–Hf isotopic studies of single zircon grains. *Chinese Science Bulletin* 50 (18), 2080–2089.
- Yu, J.H., Wang, L.J., Wei, Z.Y., Sun, T., Shu, L.S., 2007. Phanerozoic metamorphic episodes and characteristics of Cathaysia Block. *Geological Journal of China Universities* 13 (3), 474–483 (in Chinese with English abstract).
- Zhang, Z.M., Liou, J.C., Coleman, R.C., 1984. An outline of the plate tectonics of China. *Geological Society of America Bulletin* 95, 295–312.
- Zhang, F.R., Shu, L.S., Wang, D.Z., Yu, J.H., Shen, W.Z., 2009. Discussion on the tectonic setting of Caledonian granitoids in the eastern segment of South China. *Earth Science Frontiers* 16 (1), 248–260 (in Chinese with English abstract).
- Zhang, F.F., Wang, Y.J., Fan, W.M., Zhang, A.M., Zhang, Y.Z., 2010. LA-ICPMS zircon U–Pb geochronology of late Early Paleozoic granites in eastern Hunan and western Jiangxi Provinces, South China. *Geochimica* 39 (5), 414–426 (in Chinese with English abstract).
- Zhang, F.F., Wang, Y.J., Zhang, A.M., Fan, W.M., Zhang, Y.Z., Zi, J.W., 2012. Geochronological and geochemical constraints on the petrogenesis of Middle Paleozoic (Kwangssian) massive granites in the eastern South China Block. *Lithos* 150, 188–208.
- Zhao, G.C., Cawood, P.A., 1999. Tectonothermal evolution of the Mayuan assemblage in the Cathaysia Block: new evidence for Neoproterozoic collisional-related assembly of the South China craton. *American Journal of Science* 299, 309–339.
- Zhao, K.D., Jiang, S.Y., Dong, C.Y., Chen, W.F., Chen, P.R., Ling, H.F., Zhang, J., Wang, K.X., 2011. Uranium-bearing and barren granites from the Taoshan Complex, Jiangxi Province, South China: geochemical and petrogenetic discrimination and exploration significance. *Journal of Geochemical Exploration* 110 (2), 126–135.
- Zhao, K.D., Jiang, S.Y., Yang, S.Y., Dai, B.Z., Lu, J.J., 2012. Mineral chemistry, trace elements and Sr–Nd–Hf isotope geochemistry and petrogenesis of Cailing and Furong granites and mafic enclaves from the Qitianling batholith in the Shi-Hang zone, South China. *Gondwana Research* 22 (1), 310–324.
- Zhao, K.D., Jiang, S.Y., Chen, W.F., Chen, P.R., Ling, H.F., 2013a. Zircon U–Pb chronology and elemental and Sr–Nd–Hf isotope geochemistry of two Triassic A-type granites in South China: implication for petrogenesis and Indosinian transtensional tectonism. *Lithos* 160–161, 292–306.
- Zhao, K.D., Jiang, S.Y., Sun, T., Chen, W.F., Ling, H.F., Chen, P.R., 2013b. Zircon U–Pb dating, trace element and Sr–Nd–Hf isotope geochemistry of Paleozoic granites in the Miao'ershan–Yuechengling batholith, South China: implication for petrogenesis and tectonic–magmatic evolution. *Journal of Asian Earth Sciences* 74, 244–264.
- Zhou, X.M., Li, W.X., 2000. Origin of Late Mesozoic igneous rocks in Southeastern China: implications for lithosphere subduction and underplating of mafic magmas. *Tectonophysics* 326 (3–4), 269–287.
- Zhou, X.M., Sun, T., Shen, W.Z., Shu, L.S., Niu, Y.L., 2006. Petrogenesis of Mesozoic granitoids and volcanic rocks in South China: a response to tectonic evolution. *Episodes* 29 (1), 26–33.